The BEST framework for the search for the QCD critical point and the chiral magnetic effect

Xin An, Marcus Bluhm, Lipei Du, Gerald V. Dunne, Hannah Elfner, Charles Gale, Joaquin Grefa, Ulrich Heinz, Anping Huang, Jamie M. Dmitri E. Kharzeev, Volker Koch, Jinfeng Liao, Shiyong Li, Karthein, Michael McNelis, Debora Mroczek, Swagato Mukherjee, Mauricio Martinez, Marlene Nahrgang, Angel R. Nava Acuna, Jacquelyn Noronha-Hostler, Oliinychenko, Paolo Parotto, Israel Portillo, Maneesha Sushama Pradeep, Scott Pratt, Krishna Rajagopal, Claudia Ratti, Gregory Ridgway, Thomas Schafer, Bjorn Schenke, Chun Shen, Shuzhe Shi, Mayank Singh, Vladimir Skokov, Dam T. Son, Agnieszka Sorensen, Mikhail Stephanov, Raju Volodymyr Vovchenko, Ryan Weller, Ho-Ung Yee, Venugopalan, and Yi Yin

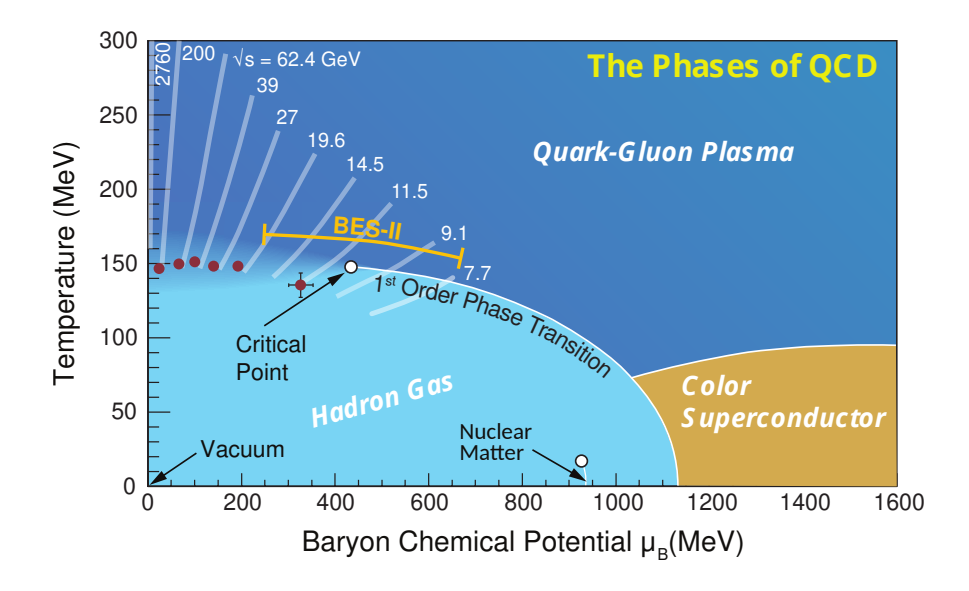
II.	Lattice QCD results	10
	A. Phase diagram	10
	B. Equation of state at nite density	11
	C. Correlations and uctuations of conserved charges	14
III.	Critical uctuations and anomalous transport	16
	A. Fluctuation dynamics near the critical point	16
	1. Introduction	16
	2. Theoretical developments	18
	B. Chiral Magnetic E ect and related phenomena	21
IV.	EoS with 3D-Ising model critical point	25

I. Introduction

V. Initial Conditions	27
A. Challenges of the Beam Energy Scan	27
B. Pre-BEST status of 3D initial condition models	28
C. Simple collision geometry based 3D initial condition	29
D. Dynamical initial condition	31
VI. Hydrodynamics	36
A. Introduction and summary	36
B. Conventional relativistic hydrodynamics	37
1. Results from full 3D dynamical simulations	37
2. Baryon di usion	41
3. Code validation for di erent hydrodynamic frameworks	42
C. Anomalous hydrodynamics	43
1. Phenomenological simulations of CME	43
2. Evolution of Electromagnetic Field	46
D. Fluctuation dynamics	47
1. Hydro+ simulations	48
2. The simulation of stochastic hydro	52
VII. Non-critical contributions to proton number uctuations	57
A. Sources of non-critical uctuations	57
1. Exact baryon number conservation	57
2. Repulsive interactions	58
3. Volume uctuations	59
B. Non-critical baseline from hydrodynamics	59
VIII. Particlization and kinetic transport	61
A. Introduction and overview	61
B. Local microcanonical particlization of uctuating hydrodynamics	65
C. Freezing out critical uctuations	67
D. Hadronic afterburner with adjustable mean- eld potentials	70
IX. Global modeling and analysis framework	74

	A. The BEST modeling framework	76
	B. Global Bayesian analysis	78
Χ.	Present Status, outlook and conclusions	81
	Note added in proof	83
	Acknowledgments	83
	References	84

The properties of hot and dense strongly interacting matter have been an important focus of research for many years. Experiments at RHIC and the LHC have revealed several interesting and unexpected properties of the Quark Gluon Plasma (QGP), most prominently its near perfect uidity [1 3], see [4, 5] for reviews. The QGP created at LHC and top RHIC energies consists in nearly equal parts of matter and antimatter, implying, in particular, that the baryon number chemical potential is much smaller than the temperature Lattice calculations [7, 8] at vanishing show that QCD predicts a crossover transition from the QGP to a hadron gas with many thermodynamic properties changing dramatically but continuously within a narrow range around the transition temperature, which lies in the interval 154 MeV 158 6 MeV [8 13]. In contrast, a droplet of QGP at large baryon number chemical potential may experience a sharp—rst order phase transition as it cools, with bubbles of QGP and hadronic matter coexisting at a well-de ned co-existence temperature. If the rst order regime exists, then the co-existence region must eventually end in a critical point. It is not yet known whether QCD has a rst order co-existence region and an associated critical point [15 21], nor is it known where in the phase diagram it might lie. Many model calculations predict the existence of a critical point, but do not reliably constrain its location (see e.g. [22] for an overview). Model-independent lattice QCD calculations, on the other hand, become more discult with increasing do not yet provide de nitive answers about the existence of a critical point. While lattice calculations have advanced significantly, both in terms of new techniques and advances in computing (see e.g. [17, 19, 23, 27]), at present only experimental measurements can answer



these questions de nitively.

In order to systematically survey the high baryon density region of the QCD phase diagram major experimental programs are under way (see e.g. [28] for an overview). In particular, the so called Beam Energy Scan (BES) at RHIC studies strongly interacting matter at di erent net-baryon densities by varying the collision energy, as illustrated in Fig. 1. Besides a general survey of the QCD matter, this energy or rather baryon-density scan aims at two potential discoveries that would have a signi-cant impact on our understanding of the QCD phase diagram:

• The discovery of a QCD critical point: If, as a function of the beam energy, the path of a heavy ion collision in the phase diagram changes from passing through the rst order co-existence line to traversing the crossover regime we expect to observe non-monotonic

behavior in various observables. The most dramatic e ects are predicted to occur in uctuation observables, as discussed in III A. Additional evidence is provided by hydrodynamic e ects on the lifetime and collective expansion of the reball controlled by the softening of the equation of state near a critical point.

• The discovery of the onset of the chirally restored phase: In chirally restored quark gluon plasma the handedness of fermions is conserved, but at the quantum level these conservation laws are modi ed by triangle anomalies. In the presence of an external magnetic eld, such as the one generated by the current of the colliding highly charged ions, these anomalies lead to novel transport e ects, in particular the chiral magnetic e ect (CME) [29–31] which predicts electric charge separation induced by an anomalous current.

Experimental results obtained during the strong phase of the BES program have already provided interesting signals (see [28] for a recent review) and, thus, have suggested that these discoveries may be possible. However, several improvements are needed in order to advance from a collection of tantalizing hints to a claim of discovery. The rst issue is that the data collected in the exploratory phase of the the RHIC beam energy scan do not have su cient statistics to claim any de nitive signals for either a QCD critical point or for anomalous transport processes. This situation is being addressed during the second phase of the RHIC BES, BESII. Second, and this is at the heart of the e ort we are reporting on here, to de nitively claim or rule out the presence of a QCD critical point or anomalous transport requires a comprehensive framework for modeling the salient features of heavy ion collisions at BES energies which allows for a quantitative description of the data. A crucial aspect of this e ort is the need to embed equilibrium quantities like the critical equation of state and anomalous conservation laws into a dynamical scheme. This framework correlates di erent observables, predicts the magnitude of the expected e ects, includes conventional backgrounds, and relates a possible discovery at a given beam energy, nuclear species and impact parameter to the existence of a phase boundary or a critical point at a location) in the phase diagram.

This task requires advances on many theoretical frontiers, ranging from lattice QCD to hydrodynamics, magnetohydrodynamics, and kinetic theory, and nally to the tasks of model validation and data analysis. Specifically, the dynamical framework which has been

developed to successfully describe the evolution of a system created at top RHIC and LHC energies needs to be extended in several key aspects:

- Initial condition: At energies relevant for the BES the colliding nuclei are not succeed to be considered thin sheets in the longitudinal direction. As a consequence, the transition to hydrodynamics does not happen at one given (proper) time but over a time interval of several fm/. Therefore, as parts of the system already evolve hydrodynamically others are still in the pre-hydrodynamic stage. In addition, at the lower collision energies the dominance of gluons in the initial state is no longer given, and quark degrees of freedom together with their conserved charges need to be taken into account.
- Hydrodynamic evolution: Viscous hydrodynamics, which has been successfully applied to the systems at the highest energies, needs to be amended to account for the propagation of the non-vanishing conserved currents of QCD: baryon number, strangeness and electric charge, together with their respective dissipative (di-usive) corrections. In addition, the description of anomalous transport requires the inclusion of anomalous currents together with their dissipative terms. Finally, in order to evolve (critical)—uctuations and correlations, one has to develop a framework that incorporates higher moments of the hydrodynamic variables, and that takes into account out-of-equilibrium e ects such as critical slowing down near a critical point, or domain formation near a rst order transition. Two approaches are currently being pursued, stochastic hydrodynamics, as well as deterministic evolution equation for second- and higher-order correlation functions.
- Equation of state: The hydrodynamic evolution of systems created at the BES requires an equation of state (EOS) at nite and possibly large net baryon number chemical potential with a potential phase transition and critical point, the location of which is still unknown. Additional dependencies on net strangeness and electric charge densities are essential to reproduce the hadronic chemistry at di erent collision energies. Therefore, one has to develop a model equation of state which includes a phase transition and which at the same time has a solid footing in QCD. To this end it is important to calculate in Lattice QCD higher order coe cients for the Taylor expansion of the pressure in terms of the baryon number chemical potential. These

will then serve QCD constraints for any equation of state with a phase transition and critical point.

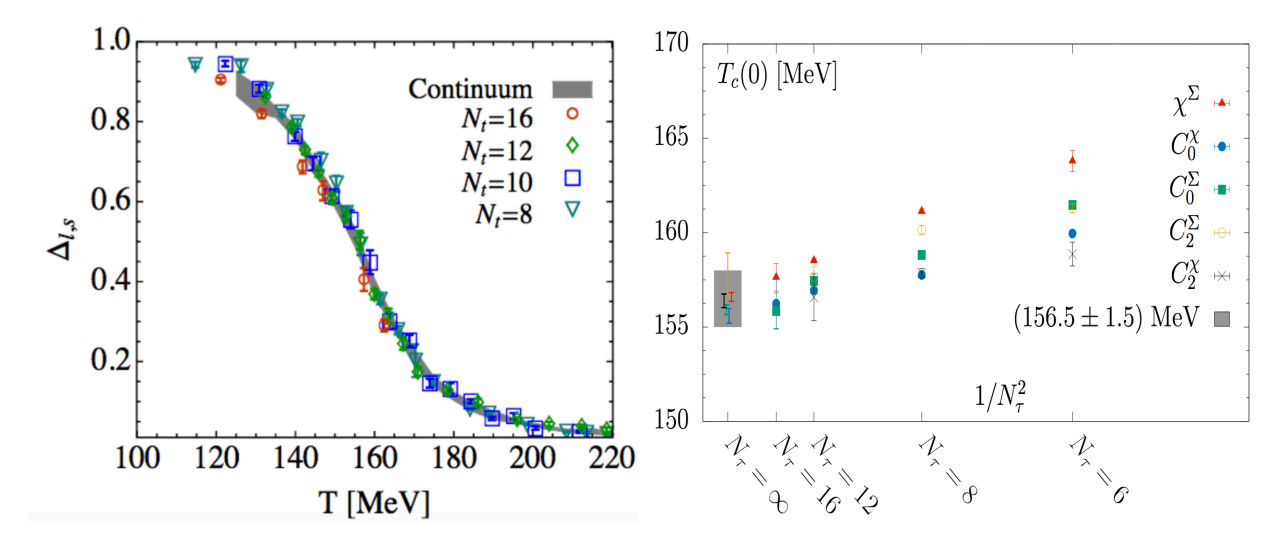
- Particlization: The transition from hydrodynamic elds into particles, often referred to as particlization, which typically is implemented at the phase boundary, needs to ensure that uctuations and correlations are preserved and do not receive additional (spurious) contributions [32].
- Hadronic phase: The relative time the system spends in the hadronic phase increases with decreasing collision energy. Therefore, the kinetic out-of-equilibrium evolution of the hadronic phase requires special attention. In addition, one needs to allow for (mean eld) interactions in order to match a possible phase transition and critical point in the hadronic phase and evolve the system in the presence of these interactions.
- Data analysis: A Bayesian global analysis, similar to that already successfully applied to the highest energy collisions [33–37], is required to constrain and extract the physical parameters of the model, such as transport coe—cients and the location of critical point etc. Since at lower energies we encounter additional relevant dynamical variables, such as di—usion coe—cients, critical point, mean—elds etc, the presently available Bayesian analysis frameworks need to be extended considerably.

It is the purpose of this paper to report on the progress made by the Beam Energy Scan Theory (BEST) Collaboration towards developing a dynamical framework which takes into account these essential new aspects. We start with an overview of the recent, pertinent, results from lattice QCD. Next we brie y review the relevant theoretical concepts with regards to critical uctuations and anomalous transport. Before we turn to the various new developments concerning the initial state and hydrodynamics we discuss the modeling of the equation of state with a critical point. After discussing several new methods for particlization and the kinetic treatment of the hadronic phase we nally present the Bayesian data analysis framework which will be applied in order to constrain the physical model parameters with experimental data.

Numerical simulations have demonstrated that at zero baryon chemical potential the QCD phase transition between hadronic matter at low temperature and a QGP at high temperature is a smooth crossover [7]. The QCD Lagrangian is symmetric under chiral transformations of the fermion elds in the case of massless quarks. However, chiral symmetry is spontaneously broken by the QCD vacuum, and the chiral condensate

$$= -\frac{\ln}{} \tag{1}$$

has a non-zero expectation value at low temperatures. Here, is the QCD partition function, is the volume, and is the mass of a quark with avor $= up \ down$. As quarks decon ne and the transition to the QGP takes place, chiral symmetry is restored. This is evident from the fact that the chiral condensate features a rapid decrease in the vicinity of the transition temperature, and approaches zero at high temperatures, see the left panel of Fig. 2.



Because of the crossover nature of the transition, a denition of the transition temperature is ambiguous. A common choice is to locate the peak of the chiral susceptibility =

as a function of the temperature. By extrapolating this observable to nite chemical potential it is possible to follow the location of the transition temperature with increasing :

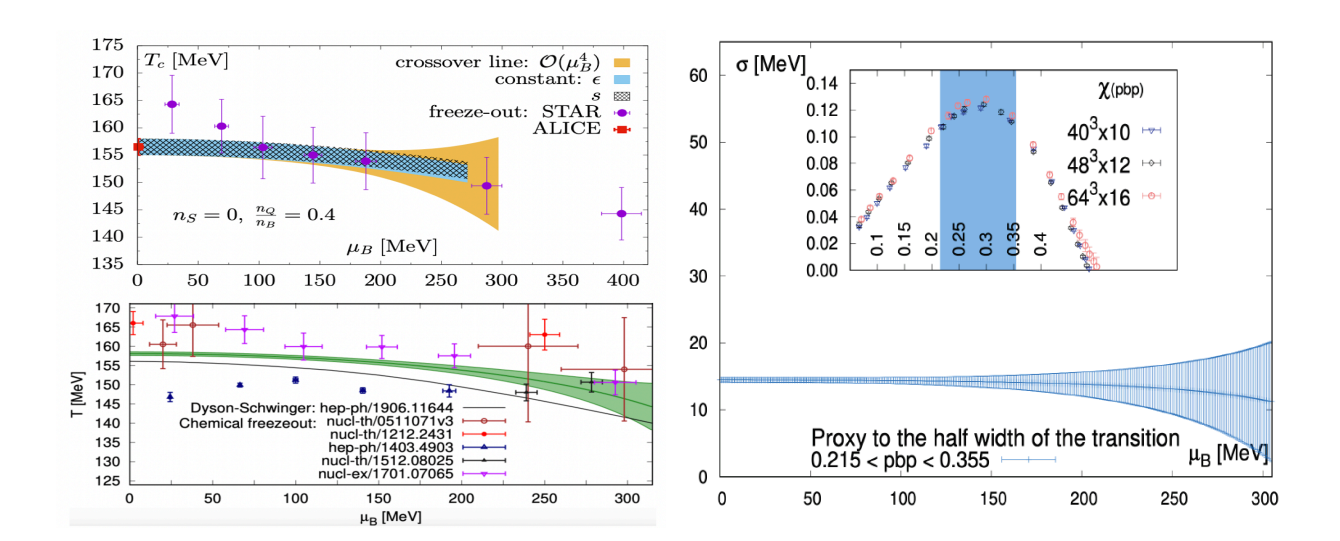
$$\frac{}{}(0) = 1 \qquad \frac{}{} + \frac{}{}(2)$$

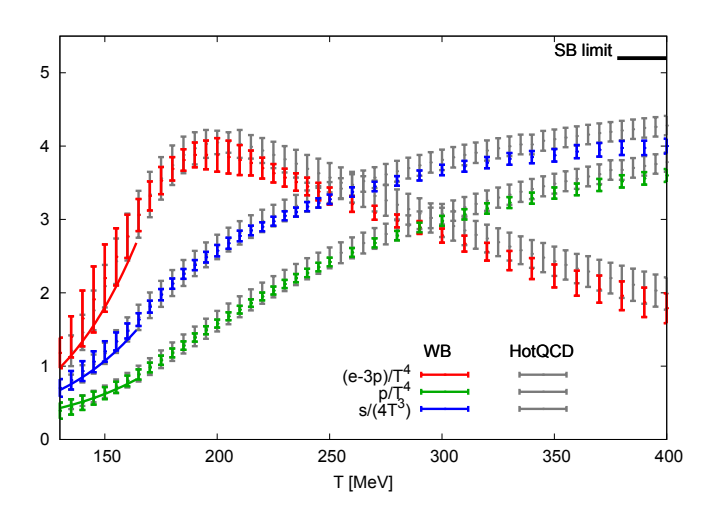
The right panel of Fig. 2 shows the pseudo-critical temperature at = 0, extrapolated to the continuum using ve di erent chiral observables to de ne its location. The state of the art results for the transition temperature at = 0 (= 156 5 1 5 MeV [12] and = 158 0 0 6 MeV [13]), the curvature of the phase diagram (= 0 012(4) [12] and = 0 0153(18) [13]) and the fourth-order correction (= 0 000(4) [12] and = 0 00032(67) [13]) have all been obtained within BEST by members of the HotQCD and WB collaborations, respectively (for previous results see Ref. [39 45], for a determination of the QCD transition temperature in the chiral limit see Ref. [46]). It is worth pointing out that the curvature is very small and that the fourth-order correction is compatible with zero; besides, the results of the two collaborations, obtained with di erent lattice actions, agree with each other within uncertainties.

The left panel of Fig. 3 shows the transition line obtained in Refs. [12] (top) and [13] (bottom). By calculating the second-order baryon number—uctuation along the transition line [27] or by looking at the height and width of the peak of the chiral susceptibility [13] it was concluded that no sign of criticality is observed in lattice QCD simulations at 300 MeV. This is evident from the right panel of Fig. 3, which shows the width of the chiral susceptibility peak as a function of the chemical potential: while a decrease is expected in the vicinity of the critical point, the curve is compatible with a constant.

The equation of state of QCD at = 0 has been known from rst principles for a number of years. The WB Collaboration published continuum extrapolated results for pressure, energy density, entropy density, speed of sound and interaction measure in Refs. [47, 48]. These results were con rmed by the HotQCD Collaboration in Ref. [11]. A comparison between these results is shown in Fig. 4.

Lattice QCD simulations at nite chemical potential are hindered by the well-known sign problem, which limits the range of available results for the thermodynamics of strongly





interacting matter. The equation of state of QCD at $\,$ nite density is obtained either as a Taylor series in powers of $\,$ around $\,$ = 0, or through simulations at imaginary

chemical potential and their analytical continuation to real [50]. The Taylor expansion of the pressure can be written as

$$\frac{()}{-} = \frac{()}{-} + \frac{1}{!} \frac{()}{(-B)} = - = () - (3)$$

where the coe cients are de ned as

$$=\frac{1}{!}\frac{()}{()}\tag{4}$$

and they are related to the susceptibilities of conserved charges as

$$= \frac{1}{!} \qquad \text{where} \qquad = \frac{()}{()} \quad \text{and} \qquad = \tag{5}$$

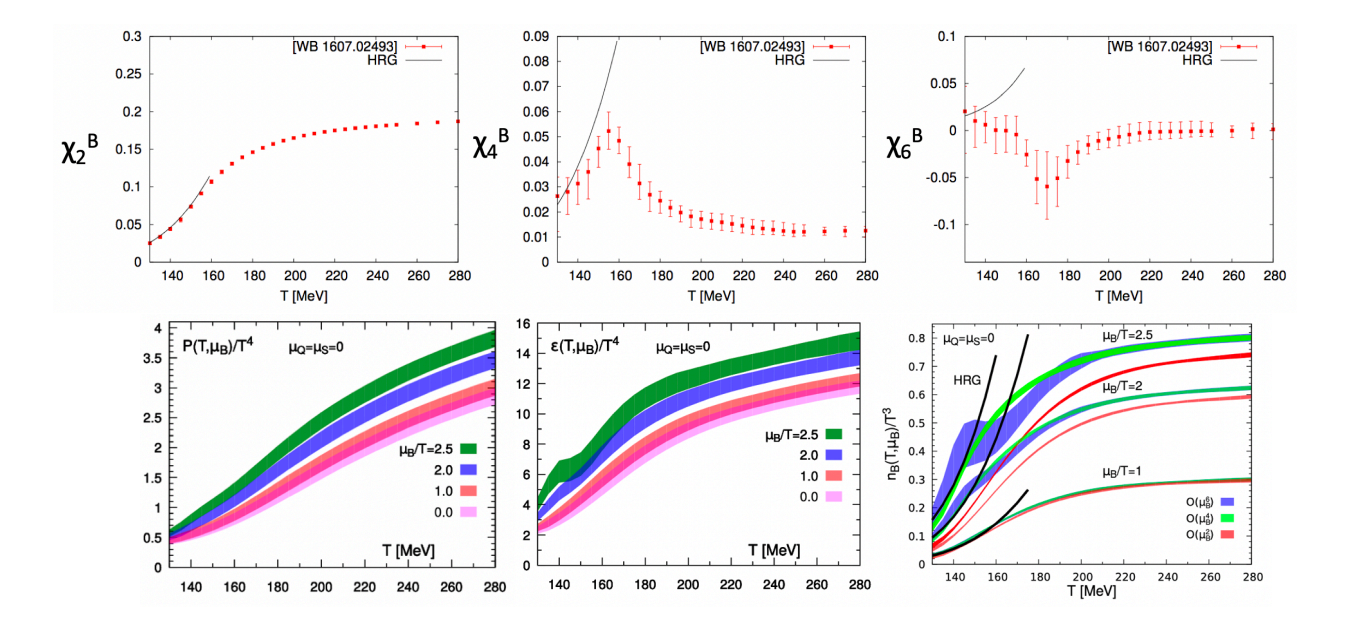
At temperatures of 100 160 MeV it is possible to make direct comparisons between a hadron resonance gas model and Lattice QCD, which show a good agreement for most observables, when using enhanced particle lists which include either barely seen [51 53] or predicted but not yet observed [54] resonant states as input.

One has to keep in mind that there are three conserved charges in QCD: baryon number and strangeness. When extrapolating to nite baryonic chemical potential, a choice needs to be made also for and . Two common choices in the literature are either =0, or and as functions of and such that the following conditions are satis ed: = 0,0.4, where is the density of conserved charge. The latter rejects the initial conditions in a heavy-ion collision, namely the proton to neutron ratio in heavy nuclei such as Au and Pb and the absence of netstrangeness in the colliding nuclei. After the early results for and [18], the rst results were published in Ref. [55]; results for continuum extrapolated were shown in Ref. [56], but only for a nite lattice spacing. The BEST Collaboration obtained the state of the art lattice QCD Equation of State at nite density in three distinct cases:

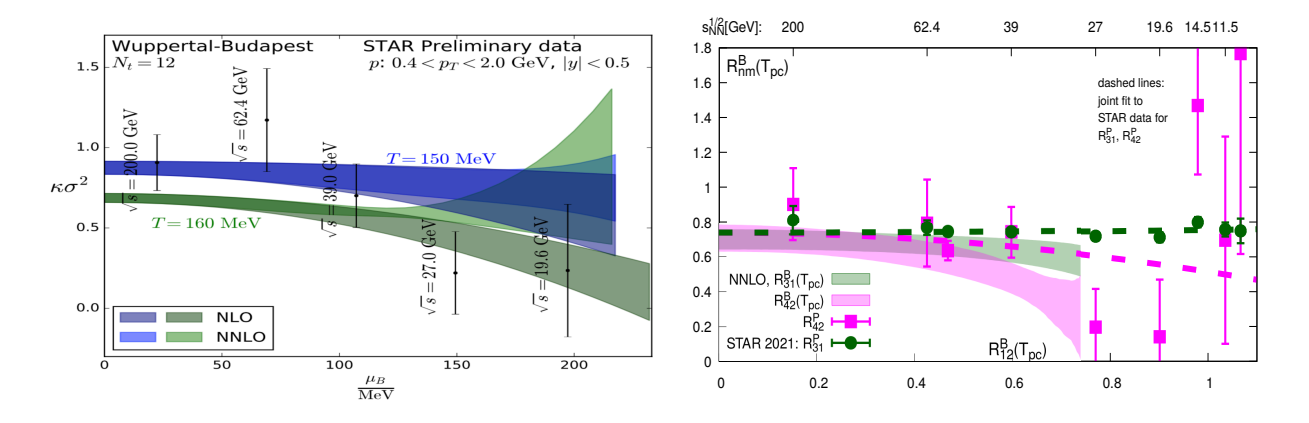
- 1. Continuum extrapolated results for the Taylor expansion coe cients of the pressure up to $\mathcal{O}(($)) in the case of =0 and =0.4 [57, 58].
- 2. Continuum extrapolated results for the Taylor expansion coe cients of the pressure up to $\mathcal{O}(($)) [59], a continuum estimate of the sixth-order coe cient [24] and results for at = 8 [60] and = 12 [61] at = 0.

3. Reconstructed equation of state, up to fourth-order in chemical potential [62], or including some sixth-order terms [63] at nite and .

Figure 5 shows the Taylor coe cients for case 1 (upper panels, from Ref. [57]) and some thermodynamic quantities for case 2 (lower panels, from Ref. [24]), respectively. More recently, a novel extrapolation method has been proposed in Ref. [64], which considerably extends the range in — and eliminates the wiggles around the transition temperature, typical of the Taylor expansion method (see the blue bands in the bottom right panel of Fig. 5).



Fluctuations of conserved charges are one of the most promising measurements from the Beam Energy Scan program, as they are sensitive to the presence of a critical point [16, 19, 65] and allow a comparison between rst principle results and experiments [66 68]. Results for uctuations at small chemical potentials and their comparison to data have been obtained in the past [69 72]. Within the BEST Collaboration, several new results for equilibrium uctuations of conserved charges have been obtained on the lattice, and comparisons to the Hadron Resonance Gas model, to perturbation theory [73, 74] and to experimental results have been discussed.

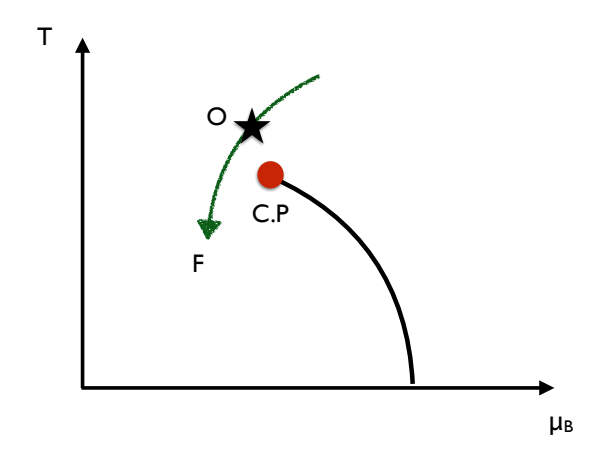


The high-temperature behavior of uctuations and correlations between di erent avors was explored in Refs. [59, 76]. In Ref. [61], several higher order diagonal and o -diagonal correlators between baryon number, electric charge and strangeness were explored. The higher order coe-cients were used to expand the lower order ones to nite chemical potential and compare them to experiment. Results for the ratio of the fourth- to second-order baryon number uctuations, from Ref. [61] are shown in the left panel of Fig. 6, in comparison to experimental results from the STAR Collaboration [75]. HADES has similar measurements at = 2 4 GeV [77]. For a determination of the curvature of the chemical freeze-out line, see Ref. [78].

The right panel of Fig. 6 shows similar results from Ref. [60]. In particular, it was pointed out in that manuscript that the observed decrease in the experimental values with decreasing collision energy can be reproduced from rst principles. One should however keep in mind that lattice QCD results correspond to the thermodynamic equilibrium uctuations of the

baryon number in the grand-canonical ensemble limit, while the experimental data show uctuations of net-protons. The relation between the two, in thermal equilibrium, has been explained in Ref. [79]. A quantitative analysis of the dierence between protons and baryons at RHIC-BES was presented in [80]

More recently, triggered by forthcoming experimental measurements from the STAR collaboration, results for baryon number—uctuations up to sixth-order at small values of have been obtained in Ref. [60]. The same motivation was behind new results for—,—, correlators at—nite chemical potential, and the de—nition of their proxies to be compared to experimental results in Ref. [81]. For recent reviews of the state of the art of—rst principle simulations in comparison to experimental results see Refs. [49, 82].



To turn high precision experimental data anticipated from BESII into de nitive information about the existence of a QCD critical point a quantitative framework for modeling the salient features of these low energy collisions is indispensable. To this end, viscous hydrodynamics, which successfully describes the evolution of the reballs created at top RHIC and LHC energies needs to be extended to be suitable for the conditions at lower energies. For example, as discussed in detail in Sec. VI the conserved currents of QCD need to be propagated explicitly. In addition, an equation of state (EOS) with a critical point in the universality class of a possible QCD critical endpoint is needed. The QCD critical point is expected to be in the 3d Ising class [83, 84]. As we shall see in Sec. IV such an EOS has been constructed in Ref. [85].

However, as the reball approaches the critical point, hydrodynamics is not su cient to capture all the relevant dynamics. In particular, the evolution of the long wavelength uctuations (LWF) of the order parameter—eld close to the critical point is beyond a hydrodynamic description. Due to critical slowing down, LWF inescapably fall out of equilibrium as the system approaches the critical point, see Fig. 7 for an illustration. An analysis of the resulting out-of-equilibrium e ect [86] (see Ref. [87] for more references) indicates that in many phenomenological relevant situations the real-time—uctuations di er from equilibrium expectations not just quantitatively, but even qualitatively. In addition, since the order parameter—uctuations themselves contribute to the stress-energy tensor—, their out-of-equilibrium dynamics back-react on the bulk evolution of the—reball. Therefore, a quantitative framework that describes the intertwined dynamics among the—uctuations near the phase boundary and bulk evolution is crucial, see [88] for a recent review. We now discuss the basic features of such a framework, and the present status of their implementation will be presented in Sec. VID.

Before turning to the quantitative framework, let us—rst explain qualitative features of critical dynamics. A key concept is Kibble-Zurek (KZ) dynamics (see Ref. [89] for a review). Since the evolution of the critical—uctuations becomes e—ectively frozen at the point where the time remaining to reach the critical point is shorter than the relaxation time (the point O—in Fig. 7), one can use the frozen correlation length, known as the KZ length,—, and the aforementioned timescale at which critical—uctuations become frozen,—, to characterize the qualitative features of out-of-equilibrium evolution near the critical point. The KZ timescale——also determines the time interval during which out-of-equilibrium e ects are important. According to the benchmark estimate presented in Ref. [90],——for a heavy-ion collision is around 6 fm. Out-of-equilibrium scaling leads to a potentially unique signature

of critical behavior, and Kibble-Zurek scaling for non-Gaussian cumulants has been studied in model calculations [91].

The study of out-of-equilibrium uctuations has already attracted much attention, prior to the works discussed here. The limitation of the growth of the critical correlation length due to nite time e ects was originally studied in Ref. [92], and the dynamic universality class (model H) of a critical point in the QCD phase diagram was identied in [93]. A number of authors investigated the theory of uctuations in relativistic uid dynamics [94–97], out-of-equilibrium e ects on non-Gaussian cumulants were investigated in Ref. [86] based on a set of cumulant equations. In parallel, the model of chiral uid dynamics (CFD) was developed [98–101] (see Ref. [102] for an overview), and extended to a QCD-assisted transport approach [103] by using an elective potential beyond meaned and the sigma spectral function from functional renormalization group calculations [104]. In the CFD framework, the chiral condensate is identied as a dynamical variable while the slow modes relevant for the QCD critical point are related to conserved baryon densities (see Refs. [93, 105, 106]). We note that the dynamics of the chiral condensate has interesting phenomenological consequences [107] and its quantitative impact on critical uctuations in full nonequilibrium calculations remains to be evaluated.

The appropriate quantitative framework for describing those out-of-equilibrium LWF modes is fluctuating hydrodynamics supplemented with the salient feature of a critical point. Fluctuating hydrodynamics describes the evolution of (average) hydrodynamic variables and their uctuations. In the traditional stochastic approach, described by Landau and Lifshitz [108], the e ects of uctuations are accounted for by adding stochastic noise terms to the conservation equations. The magnitude of the noise, encoded in noise correlation functions, is xed by the uctuation-dissipation theorem. This approach has been extended to relativistic hydrodynamics in Ref. [97]. Even though numerical simulations based on the stochastic approach are computationally demanding, we shall discuss encouraging new progress along this direction in Sec. VI.

In contrast to the more familiar stochastic approach, the same dynamics may also be captured in a deterministic approach [90, 109–118]. In this approach, wavenumber-dependent

correlation functions of hydrodynamic variables are treated as additional slow variables in addition to the hydrodynamic ones. The resulting equations of motion are deterministic and describe the coupled evolution of the correlation functions and the conventional hydrodynamic variables. This approach successfully describes several non-trivial out-of-equilibrium e ects. For example, the authors of Ref. [112] studied the impact of hydrodynamic uctuations on correlation functions in a uid with a conserved charge (such as baryon charge) undergoing a scaling (Bjorken) expansion. In Ref. [113], the deterministic approach is extended for a general uid background. Simulations using the deterministic approach are less computationally demanding than those based on stochastic hydrodynamics, because the equations of motion are similar in structure to those of ordinary uid dynamics. First applications for 3-dimensionally expanding systems, albeit with residual symmetry constraints, were reported in [117, 118]. However, the deterministic approach becomes more and more complex if one wants to go beyond two-point functions, as would be required in order to study non-Gaussian uctuations.

The Hydro+ formalism, which we will discuss in more detail, follows the deterministic approach. Hydro+ was developed to describe the intertwined dynamics of critical uctuations and bulk evolution [111]. The key new ingredient in Hydro+ is the Wigner transform of the equal-time (in the LRF) two-point function of the uctuation of the order parameter eld (x):

$$\mathbf{q}(\mathbf{x})$$
 \mathbf{y} $(\mathbf{x} \mathbf{y} 2)$ $(\mathbf{x} + \mathbf{y} 2)$ $\mathbf{y} \mathbf{Q}$ (6)

Here, $\mathbf{q}(\mathbf{x})$ describes the magnitude of the critical uctuation at wavelength 1, and depends on time and spatial coordinate \mathbf{x} . The quantity $\mathbf{q}(\mathbf{x})$ is treated as a dynamical variable in Hydro+ and obeys a relaxation rate equation:

$$+ \qquad \mathbf{Q}(\quad) = \quad \mathbf{Q} \quad \mathbf{Q}(\quad) \qquad \mathbf{Q}(\quad) \tag{7}$$

where Q is the equilibrium value of Q. The stress-energy tensor and baryon number current are still conserved, and their conservation equations, Q = 0 and Q = 0, together with Eq. (7) are the equations of motion for Hydro+. However, the transport coe cients and EOS are generalized in Hydro+. In particular, the constitutive relation for is given by:

$$=$$
 + $($ + $)$ + viscous terms (8)

with a similar expression for $\,$, see Ref. [111]. Note that the generalized pressure depends not only on the hydrodynamic variables $\,$ and $\,$, the energy and baryon number densities, but also on the additional Hydro+ variable $\,_{\boldsymbol{Q}}(\,\boldsymbol{x})$. is related to the generalized entropy density $\,$ by generalized thermodynamic relations [111]. Since hydrodynamic (collective) $\,$ ow is induced by the gradient of the generalized pressure, in Hydro+ the bulk evolution is intrinsically coupled with that of $\,_{\boldsymbol{Q}}(\,\boldsymbol{x})$. Therefore, Hydro+ couples LWF with hydrodynamics self-consistently.

Before closing this discussion, we would like to mention that the application of the deterministic approach is not limited to studying critical—uctuations. For example, the evolution of the—uctuations of conserved charges was investigated in Refs. [115, 116, 119] in order to constrain the charge di—usive constant of the quark-gluon plasma from balance function measured experimentally at top RHIC energy. In Ref. [113], a general description of uctuating hydrodynamics based on the deterministic approach has been formulated. This framework matches the Hydro+ description of—uctuations near the QCD critical point and non-trivially extends inside and outside the critical region (see also Du et al. [120] for a related analysis of critical baryon di—usion e—ects). Finally, we note that with suitable generalizations, the formalism of Hydro+ can also be used to study hydrodynamics with chiral anomaly which couples non-conserved axial charge densities to hydrodynamic modes.

In spite of the signi cant progress made with regards to the evolution of LWF there is still need for further development:

- 1. The formalism of uctuating hydrodynamics discussed in this section only applies to the crossover side of the phase boundary. How to extend this to the rst order transition region requires further investigation. The authors of Refs. [121–123] have investigated the role of the spinodal instability based on hydrodynamics with an EOS that contains a rst order transition as well as a nite range term to model the interface tension. However, it remains to be investigated how these results are a ected by critical and non-critical uctuations.
- 2. Most of the studies based on the deterministic approach are limited to two-point functions of uctuations. The extension of the existing formalism to higher-point functions, perhaps following the method of Ref. [86], is desirable, see Ref. [124] and Ref. [114] for recent developments along this direction.

3. The additional, deterministic variables as propagated in Hydro+ are already averaged quantities and as such cannot directly be included into standard event generators of heavy-ion collisions. Additional modeling of how to couple the initial state—uctuations is necessary. Final state—uctuations, di usion and dependence on kinematic cut as occurs in the hadronic phase need to be modeled and coupled consistently. A model for particlizing, or freezing out, a hydrodynamic—uid with—uctuations as described by Hydro+ is described in Sect. VIII C.

We shall report the rst simulations of Hydro+ in Sec. VI, where we also report progress using the stochastic approach.

As already discussed in Sec. II A, the spontaneous breaking of chiral symmetry by the formation of a chiral condensate in the vacuum is a fundamental feature of QCD. An equally important prediction of QCD is that the chiral condensate will eventually disappear at high temperature, and that chiral symmetry is restored. Chiral restoration above a critical temperature 155MeV has been established by lattice QCD calculations [8, 38]. The system created in heavy ion collisions at RHIC and LHC is expected to reach the chiral transition temperature and it is important to devise a measurement that directly probes chiral symmetry restoration.

A promising approach is to look for the so-called Chiral Magnetic E ect (CME) [29–31] which predicts the generation of an electric current by an external magnetic eld under the presence of chirality imbalance:

$$\mathbf{J} = \frac{}{2} \mathbf{B} \tag{9}$$

where the sum is over all light avors with electric charge , and is the axial chemical potential that quanti es the chirality imbalance i.e. the di erence in densities between right-handed and left-handed quarks. The CME is an important example of anomalous chiral transport processes.

The CME requires a chirality imbalance (i.e. = 0). In the initial state of a heavy ion collision such an imbalance can arise from topological transitions in the gluon sector, such as

instantons and sphalerons. These objects are a key feature of non-perturbative dynamics in QCD, but they are hard to observe directly, because gluons do not carry conserved quantum numbers such as baryon number or electric charge. The QCD axial anomaly implies that every topological transition in the gluon sector induces a change in the chirality by 2 units. Consequently, an experimental observation of chirality imbalance via the CME would also be a direct probe of the elusive gluon topological transitions.

The CME also requires that the chirality imbalance, once created by topological transitions, is not destroyed by explicit or spontaneous chiral symmetry breaking in QCD. Explicit symmetry breaking is encoded in current quark masses, while spontaneous symmetry breaking is related to the quark condensate and the so-called constituent mass 300 MeV. Both e ects correspond to operators that violate chirality by two units. While the e ect of a small current quark mass on the CME is negligible, the e ect of a constituent mass is not. For this reason, the observation of the CME can provide important evidence for chiral symmetry restoration.

In addition to the CME, there are other anomalous chiral transport phenomena such as the so-called Chiral Vortical E ect (CVE) [125–128], the Chiral Electric Separation E ect (CESE) [129, 130] as well as the Chiral Magnetic Wave (CMW) [131, 132]. These ideas have attracted strong interdisciplinary interest, particularly in condensed matter physics (for a review see [133]). For a more detailed discussion and an extensive bibliography, see the recent reviews [28, 134–140].

While the scienti c signi cance of a possible CME discovery is high, the experimental search has encountered considerable challenges since the program was initiated in 2004 [29, 141]. The key issues were identified at the start of the BEST Collaboration around 2015. The past several years have seen significant progress in addressing these issues, as well as new opportunities for experimental signatures, as we discuss next.

For the CME to occur in heavy ion collisions requires a net axial charge — in a given event, as well as a strong magnetic—eld. Let us—rst discuss the axial charge generation. In a typical collision the—reball acquires considerable initial axial charge — from random topological—uctuations of the strong initial color—elds. This has been demonstrated by recent classical-statistical simulations performed in the so-called glasma framework [142–146], which provides a quantitative tool for constraining the axial charge initial conditions that would be necessary for evaluating CME signals in these collisions.

Axial charge is not conserved due to the quantum anomaly and the nonzero quark masses. That is, starting with a certain non-vanishing initial —, it will subsequently relax toward a vanishing equilibrium value. The rate for such relaxation is controlled by the random gluonic topological—uctuations at—nite temperature and also receives contribution from nite quark masses. Here the key issue is whether the initial axial charge can survive long enough to induce a measurable CME signal. Realistic estimates including both gluonic and mass contributions to axial charge relaxation [147–150] suggest that the QGP maintains its nite chirality for a considerable time. For the CME modeling, it is important to account for such non-equilibrium dynamics of axial charges. One approach is chiral kinetic theory, which has recently been developed [151–168], and applied to the phenomenology of heavy ion collisions in Refs. [169–172]. Alternatively, one can adopt the stochastic hydrodynamic description for axial charge dynamics [149], which can be naturally integrated into a hydrobased modeling framework for both the bulk evolution and the CME transport.

The other key element is the magnetic eld **B**. Heavy ion collisions create an environment with an extreme magnetic eld at least at very early times which arises from the fast-moving, highly-charged nuclei. A simple estimate gives $\mathbf{B} = \frac{EM}{A}$ at the center point between the two colliding nuclei upon initial impact. Given a magnetic eld of this strength and a chiral QGP, we expect the CME to occur. However, for a quantitative analysis of possible CME signals, two crucial factors need to be understood: the azimuthal orientation as well as time duration of the magnetic eld. A randomly oriented magnetic eld which is not correlated to any other observable such as elliptic ow prevents the CME, even if present, to be observed in heavy ion experiments. A magnetic eld which, although very strong initially, decays too fast would lead to an undetectably small signal [173].

As rst shown in [174, 175], strong uctuations of the initial protons in the colliding nuclei lead to significant uctuations in the azimuthal orientation of the **B** eld relative to the bulk matter geometry. Fortunately one can use simulations to quantify the azimuthal correlations between magnetic eld and various geometric orientations (e.g. reaction plane, elliptic and triangular participant planes) in the collision. Such magnetic eld uctuations turn out to be useful features for experimental analysis, by comparing relevant charge-dependent correlations measured with respect to reaction plane as well as elliptic and triangular event planes, see the discussions in [28, 136, 139].

The strong initial magnetic eld rapidly decays over a short period of time due to the

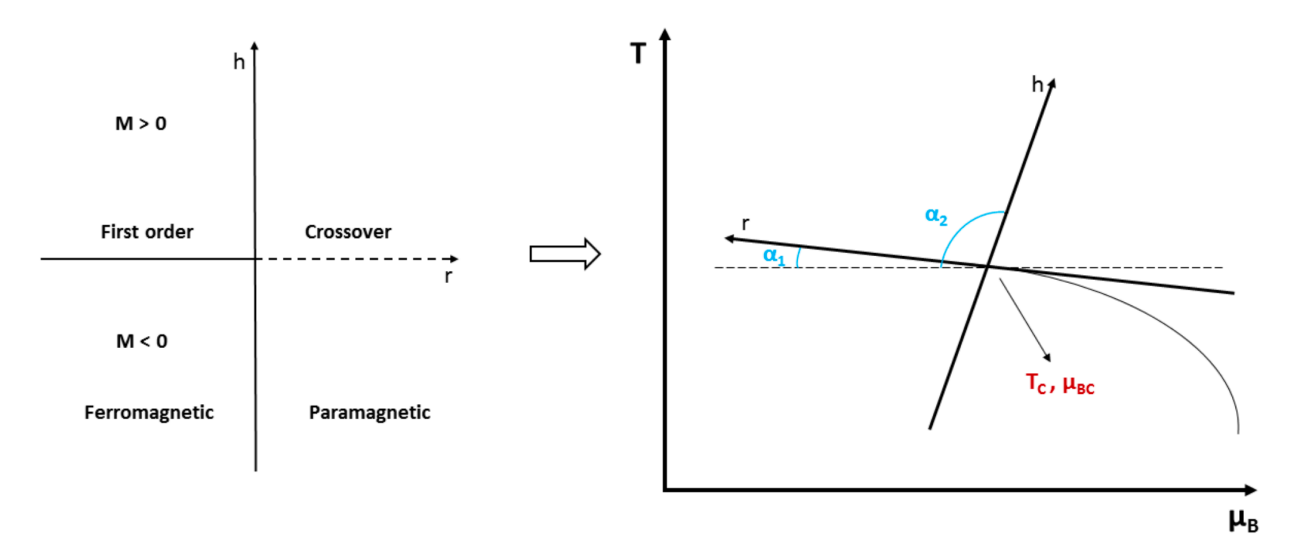
rapid motion of spectator protons along the beam direction. Understanding the dynamical evolution of the residual magnetic eld in the mid-rapidity region is a very challenging problem. Many studies based on different levels of approximation have been made [176–185]. Generically we expect an electrically conducting QGP to increase the lifetime of the **B** eld, but quantitative determinations are different cult. Simulations were performed based on a magneto-hydrodynamic (MHD) framework [178, 179, 186–190]. However the QGP may not have a sufficiently large electric conductivity to be in an ideal MHD regime. Another, perhaps more realistic approach aims to solve the in-medium Maxwell's equations in an expanding and conducting uid while neglecting the feedback of the **B** eld on the medium bulk evolution [180]. The BEST Collaboration e orthas focused on developing a robust simulation framework for **B** eld evolution along this latter approach, with significant progress achieved recently. See further discussions in Sec. VI C. Additionally, there are interesting studies of other e ects induced by a strong magnetic eld which could be used to constrain the in-medium **B** eld in heavy ion collisions [179, 180, 183–185, 191–197].

On the experimental side, the CME-induced transport is expected to result in a dipole-like charge separation along **B** eld direction [29], which could be measured as a charge asymmetry in two-particle azimuthal correlations [141]. Extensive searches have been carried out over the past decade to look for this correlation by the STAR Collaboration at the Relativistic Heavy Ion Collider (RHIC), as well as by ALICE and CMS Collaborations at the Large Hadron Collider (LHC) [141, 198 203]. Encouraging hints of the CME have been found, in particular in the regime studied by the RHIC Beam Energy Scan program. However, the interpretation of these data remains inconclusive due to signic cant background contamination. For a more in-depth discussions see, e.g. [28, 135, 136, 138, 204]. A new opportunity of potential discovery for the CME is provided by a decisive isobar collision experiment, carried out in the 2018 run at RHIC [134, 205 208], whose data are still being analyzed.

Critical to the success of the experimental program is a precise and realistic characterization of the CME signals as well as backgrounds in these collisions. To achieve this requires a framework that addresses the main theoretical challenges discusses above: (1) dynamical CME transport in the relativistically expanding viscous QGP—uid; (2) initial conditions and subsequent relaxation for the axial charge; (3) co-evolution of the dynamical magnetic—eld with the medium; (4) proper implementation of major background correlations. A frame-

work that addresses most of these e ects, dubbed EBE-AVFD (Event-By-Event Anomalous-Viscous Fluid Dynamics) [173, 209, 210], has been developed by the BEST Collaboration and will be discussed in detail in Sec. VI C.

Starting from the results discussed above, a family of Equations of State was created, each one containing a critical point in the 3D Ising model universality class, and constrained) [85]. Earlier, an equation of state to reproduce the lattice QCD results up to $\mathcal{O}($ containing a 3D Ising model critical point was obtained in Refs. [211, 212], but the critical e ects were built on top of a quasi-particle, MIT bag or Hadron Resonance Gas model equation of state, rather than systematically matching them to lattice QCD results. In our work the mapping between the Ising model phase diagram (in terms of reduced temperature and magnetic eld) and the QCD one (in terms of and) is performed in terms of six parameters: the location of the critical point (), the angles and that the = 0 QCD one, and the (axes form with the) parameters that indicate a global and a relative scaling of the axes. Such a mapping is shown in Fig. 8.



Two of these parameters are xed imposing that the critical point lies on the phase transition line obtained in lattice QCD simulations (see details on the QCD transition line in

Section II A). The other four parameters can be freely varied by the user, who can download the code from the BEST Collaboration repository [213]. The goal is then that a systematic comparison between the predictions of hydrodynamic codes that use this EoS as an input and the experimental data, will help to constrain these parameters, including the location of the critical point.

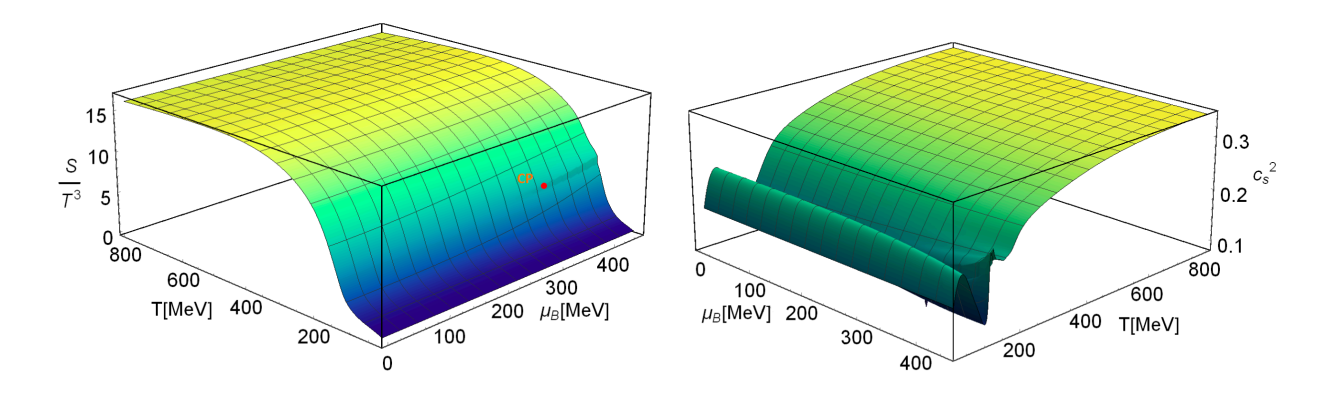
The assumption is that the lattice QCD Taylor expansion coe cients can be written as the sum of the Ising contribution and a non-critical one, that can be obtained as the di erence between lattice and Ising:

$$(\) = (\) + (\)$$
 (10)

The full pressure is then reconstructed as

$$() = () - + ()$$
 (11)

Figure 9 shows the entropy density and the speed of sound for the parameter choice used in Ref. [85]. This equation of state has been recently extended to the phenomenologically



relevant case of strangeness neutrality and xed electric charge/baryon number ratio in Ref. [214]. Recently, the BEST EoS has been used to study the behavior of the critical fourth-order cumulant of baryon number on conjectured freezeout trajectories in the QCD phase diagram [215]. It was found that subleading and non-singular terms have a signicant electron the behavior of the fourth order cumulant (kurtosis). The original prediction based on

Ising universality is that, as the baryon chemical potential increases along the freezeout curve, the kurtosis rst exhibits a dip, followed by a peak [216]. However, when subleading terms are taken into account, the dip is not a robust feature of the kurtosis along the freezeout line, and only the enhancement is a generic feature of the equation of state.

At the highest RHIC energies and at the LHC, the approaching nuclei are highly Lorentz contracted. At top RHIC energy the nuclei pass through one another in less than 0.15 fm/, and at the LHC the time is even shorter. Particles are produced over a range of rapidities, roughly de ned by the beam rapidities, 5 4 at RHIC and 8 at the LHC. This large rapidity range implies that comoving observers within one unit of rapidity around central rapidity see essentially the same physics, strongly Lorentz contracted, highly excited, target and projectile nuclei receding at a velocity close to the speed of light. This observation motivated Bjorken to propose a hydrodynamic model [217] of relativistic heavy ion collisions based on longitudinal boost invariance. The Bjorken model allows us to reduce the 3+1 dimensional evolution to a 2+1 dimensional problem. This approximation appears to hold at the 5\% level for the highest RHIC energies, when considering mid-rapidity measurements. The variation of the baryon density with rapidity can also be ignored at these energies. For a given beam energy the initial state for hydrodynamics can be characterized by 6 parameters describing the magnitude and shape of the transverse energy density pro le, the baryon density, the anisotropy of the initial stress-energy tensor, and the initial transverse ow [218, 219].

At BES energies none of these simplications are warranted. Nuclei require up to 4 fm/ to pass through one another, and a signicant fraction of the transverse collective ow has developed before the incoming nuclei have nished depositing energy. The deposition of energy and baryon number vary over a much smaller rapidity range, invalidating any assumptions of boost invariance. Describing the initial state for hydrodynamics is much more dicult as one must quantify the variations of energy density, baryon density, and initial transverse ow with rapidity. Further, one must account for the fact that energy and baryon density are deposited over a signicant amount of time [220]. Without a doubt,

modeling this phase of the collision is one of the most daunting challenges faced by the BEST Collaboration. In the next section, the status of the Pre-BEST 3D collision models is reviewed. The following two sections then present two schemes developed by the BEST Collaboration that address the challenges described above.

We present a brief summary of available models that have been or can be used to provide initial conditions for 3+1 dimensional hydrodynamic simulations. First 3+1D hydrodynamic simulations were performed with smooth initial conditions, and the typical approach to include a longitudinal structure to a transverse optical Glauber model geometry was to apply an envelope function consisting of a plateau around space-time rapidity zero and two half-Gaussians in the forward and backward directions [221]. The parameters of the model, i.e., the plateau and Gaussian widths, could then be tuned to t experimental data. The same method could also be used when uctuations in the transverse geometry are included (see e.g. [222]). Another approach, that similarly factorizes the transverse from the longitudinal dependence, was followed in [223], extending the Trento model [219] to three dimensions.

Early simulations of 3+1D hydrodynamics with initial state—uctuations in all three dimensions were performed using UrQMD [224, 225] or NEXUS [226] to provide the initial conditions [227–230]. When using UrQMD, for example, all produced point-like particles are assigned a 3D spatial Gaussian with a tuneable width to generate smeared out energy, baryon, and momentum densities as input for the hydrodynamic equations [227].

Also AMPT [231], which is based on HIJING [232], has been used to generate—uctuating initial conditions for 3+1D hydrodynamics. Here, one has mini-jets and soft partons (from melted strings) with varying formation times. Typically, after running AMPT s parton cascade, one can determine a proper time surface on which most partons have formed, use it as the initial time for hydrodynamics, and neglect late time interactions in the cascade, that occur mainly at forward rapidities [233]. Each parton is then treated similarly to the UrQMD case above and 3D Gaussians are assigned to form an energy momentum tensor in every hydro grid cell.

Aside from these models, which are based on generators that initially produce hadrons, several other options are available, including some that are based on the AdS/CFT cor-

respondence [234]. These can provide initial conditions for energy and momentum [235], as well as baryon densities [236], but so far they typically neglect geometric uctuations. Another possibility that has been explored is to extend the color glass condensate based models to three dimensions. This has been done, for example, by employing JIMWLK evolution [237–243] to determine the Bjorken—dependence of the gluon distributions in the incoming nuclei, and from that deduce the rapidity dependence [244] of the initial energy momentum tensor, or by fully extending the Yang-Mills computations, done in 2D in the IP-Glasma model [245, 246], to three dimensions [247, 248]. While these models provide an initial energy momentum tensor, baryon stopping in a saturation framework was separately addressed in [249, 250].

Except for the implementations discussed in [251] and [252], the models discussed above do not address the issue of the relatively long overlap time of the two colliding nuclei at low beam energies, which makes an initialization on a constant eigentime surface problematic. Indeed, up to now, even initial conditions based on UrQMD are based on particles propagated to a constant eigentime surface, at which hydrodynamics is initialized [230]. Within BEST, a fully dynamical initial state model, based on string deceleration, which provides three dimensional source terms for energy, momentum, and baryon currents, was developed and is implemented dynamically into the 3+1 dimensional MUSIC code [222, 253, 254]. Its advantages over existing models that have been coupled to hydrodynamics are that energy (and charge) deposition is linked to the dynamical deceleration of the string ends, which leads to a realistic space time picture, and that the model only requires a limited number of parameters, so that it can be incorporated into a Bayesian analysis framework. We will discuss this model in Section VD. In the following, we rst describe another new development, a minimal extension of the conventional Glauber model, that describes the longitudinal structure of the initial state based on energy and longitudinal momentum conservation arguments.

The conventional Glauber model assumes the colliding nuclei to be in nitely Lorentz contracted along the beam direction. The produced energy/entropy densities in the transverse plane depend on the nuclear thickness functions and . The authors of Ref. [255, 256]

proposed a minimal extension of the Glauber model to 3D which respects the constraints imposed by energy and momentum conservation locally at every transverse position in the collision. At any point in the transverse plane (), conservation of energy () and longitudinal momentum () imply that

$$() = [() + ()] \cosh() = () (12)$$

and

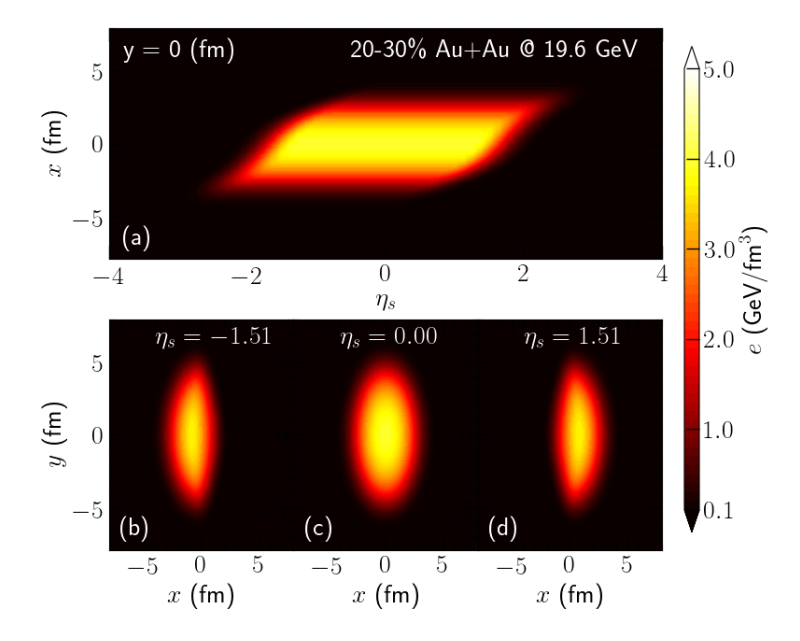
$$() = [()) ()] \sinh() = () (13)$$

respectively. Here, () are the components of the stress tensor at transverse position (), proper time , and spatial rapidity . These relations ensure that the space-momentum correlations in the initial state are continuously passed to the hydrodynamic phase. Assuming Bjorken ow, the local energy-momentum tensor of the uid at the hydrodynamic starting time matches with the Glauber model collision geometry, and especially the global angular momentum is smoothly mapped from the colliding nuclei to the uid elds.

Ref. [255] shows that at su ciently high collision energies a ux-tube-like parameterization of the longitudinal distribution of energy density () = (), combined with local energy-momentum conservation, results in a transverse energy density scaling () () (), which is preferred by the Bayesian statistical analysis [33].

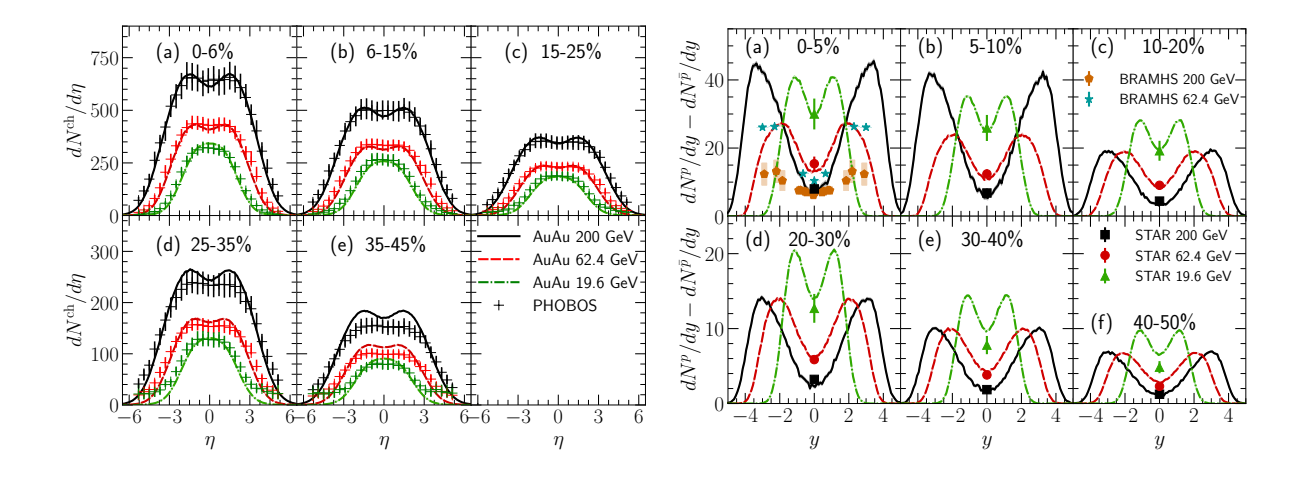
Fig. 10 shows projections of the 3D initial energy density distribution in 20-30% Au+Au collisions at 19.6 GeV. In Panel (a), the energy density is shifted to positive for 0, which is a consequence of longitudinal momentum conservation. Along the impact parameter direction (positive), the local nucleus thickness function of the projectile nucleus is larger than that of the target, which leads to a positive net longitudinal momentum in the 0 region. Panels (b-d) illustrate the shape of the energy density in the transverse direction for three di erent space-time rapidities. The reball becomes more eccentric in the forward and backward directions compared to the energy density pro le at mid-rapidity. The dipole-deformation of the reball is odd in the space-time rapidity, correlated with the direction of net longitudinal momentum .

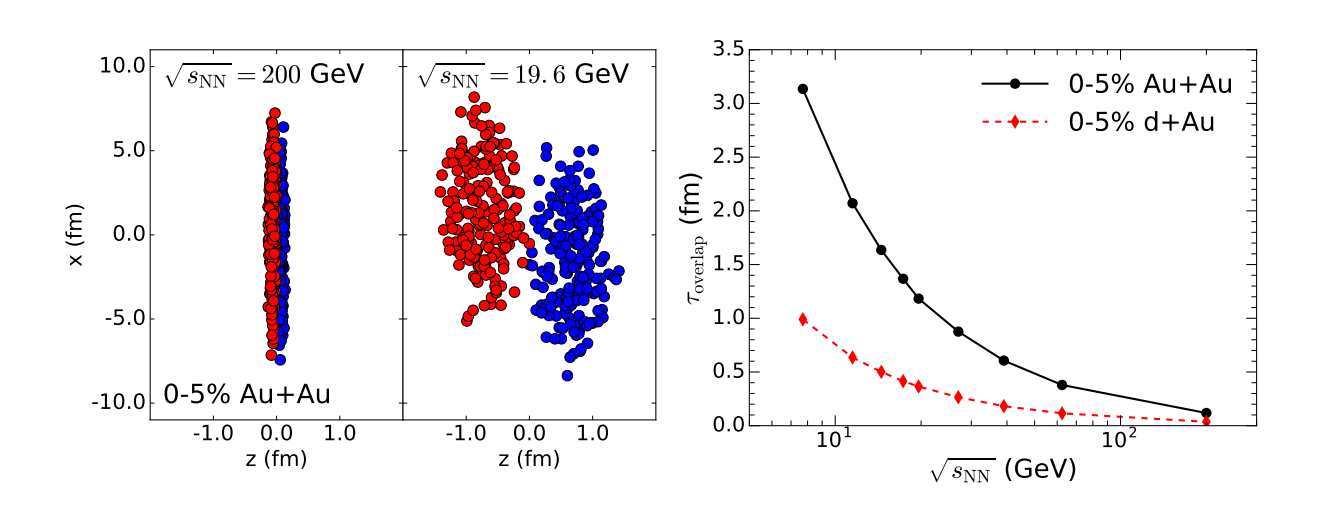
Fig. 11 shows that the collision-geometry-based initial state model with hydrodynamics + hadronic transport simulations can achieve a good description of the (pseudo-)rapidity



distributions of the produced charged hadrons and net protons measured at RHIC. Note that this model was calibrated only with the data in the most-central collisions in panel (a). The results in other centrality bins were model predictions. The rapidity evolution as a function of collision centrality was well captured by this model. For the net proton rapidity distribution, this model gives a good description of the experimental measurement at mid-rapidity as a function of centrality, while the rapidity dependence still has room for improvements.

As already noted, when the collision energy is decreased to $\mathcal{O}(10)$ GeV, the relativistic Lorentz contraction factors of the colliding nuclei along the beam (longitudinal) direction are no longer large. The overlap time required for the two colliding nuclei to pass through each other becomes signi-cant compared to the total lifetime of the system, which is of the order 10 fm $\,$, see Fig. 12. The nucleon-nucleon collision pairs that collide early will produce energy-momentum currents that evolve (possibly hydrodynamically) before the rest of the





nucleons collide with each other.

To deal with this situation, a new dynamical framework which connects the preequilibrium stage of the system to hydrodynamics on a local collision-by-collision basis was proposed [261]. The hydrodynamic evolution starts locally at a minimal thermalization time after the rst nucleon-nucleon collision. The sequential collisions between nucleons that occur later contribute dynamically as energy and net-baryon density sources to the hydrodynamic simulations.

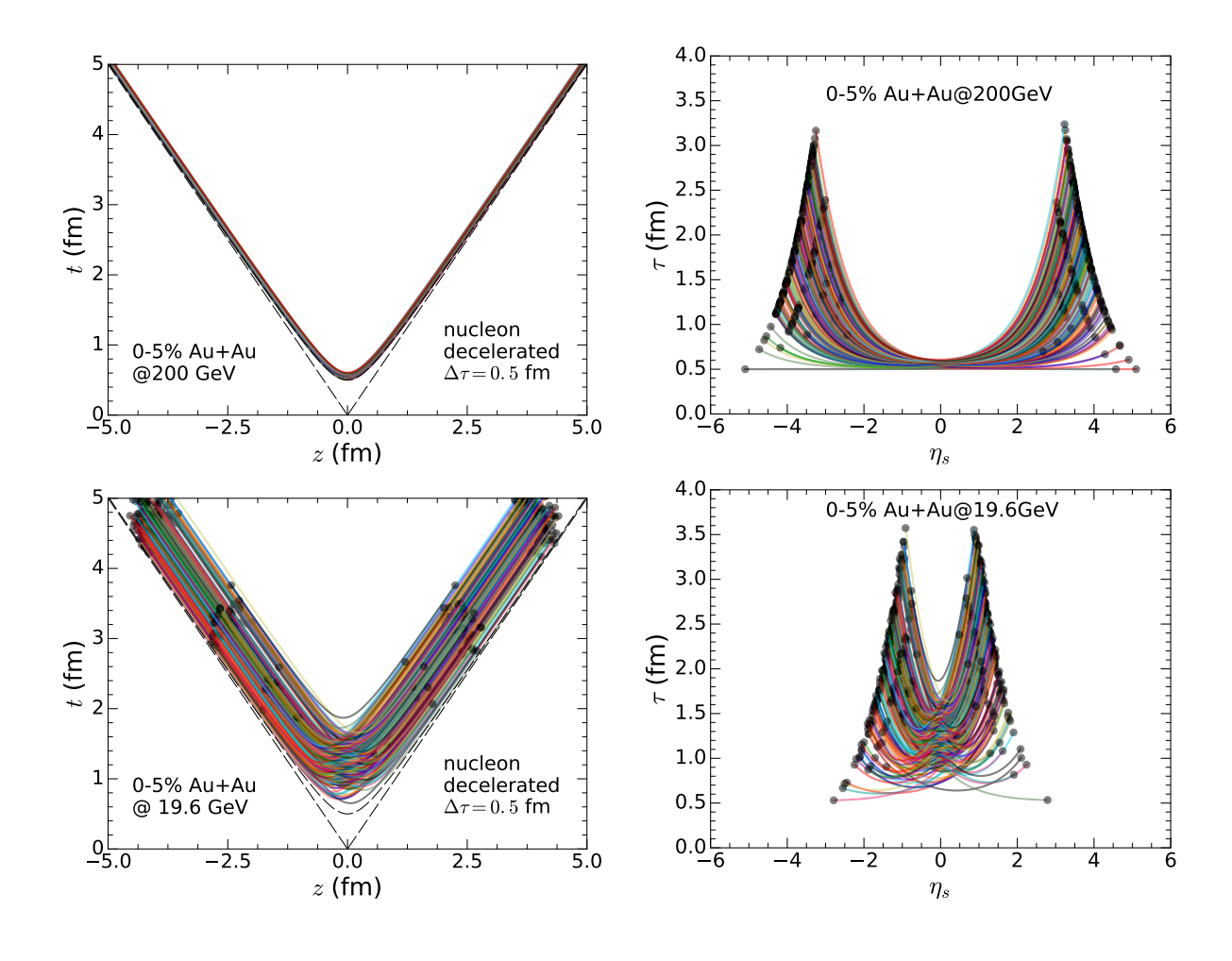
For nucleon-nucleon collisions we consider energy loss of the valence quarks, whose initial momentum fraction is sampled from nuclear parton distribution functions. They go through a classical string-deceleration model, which generates correlations between space-time and momentum.

Going beyond the BEST-developed model discussed in [261], more recent developments take into account that the energy and momentum deposited in the medium are equal to the energy and momentum lost in the deceleration process, resulting in exact energy and momentum conservation in the model. Furthermore, baryon number is propagated with some probability along the string towards midrapidity, following the idea of baryon junctions rst put forward in [262]. Consequently, the model includes spatial—uctuations of the net baryon density and energy density, and thus—uctuations of where in the phase diagram the hydrodynamic evolution begins for every position in space.

In Fig. 13 we illustrate the space time distribution of the sources that enter the hydrodynamic calculation, by showing the distributions of strings in the (left panels) or (right panels) plane for $\dot{} = 200\,\mathrm{GeV}$ (upper panels) and $\dot{} = 19\,6\,\mathrm{GeV}$ (lower panels) collisions. While at the higher energy strings are distributed close to what looks like a constant surface in the plane, there is a large spread in the direction for the lower energy collision. Studying the distribution in the plane reveals that while around midrapidity the high energy result is indeed well approximated by the assumption of a xed initial, at large space time rapidity even the high energy collision shows a significant spread in the direction. This indicates that dynamic sources are relevant for all collision systems, if one is interested in the physics beyond midrapidity. For low collision energies, there is no way around the fact that the initial energy deposition takes a significant amount of time, even at midrapidity.

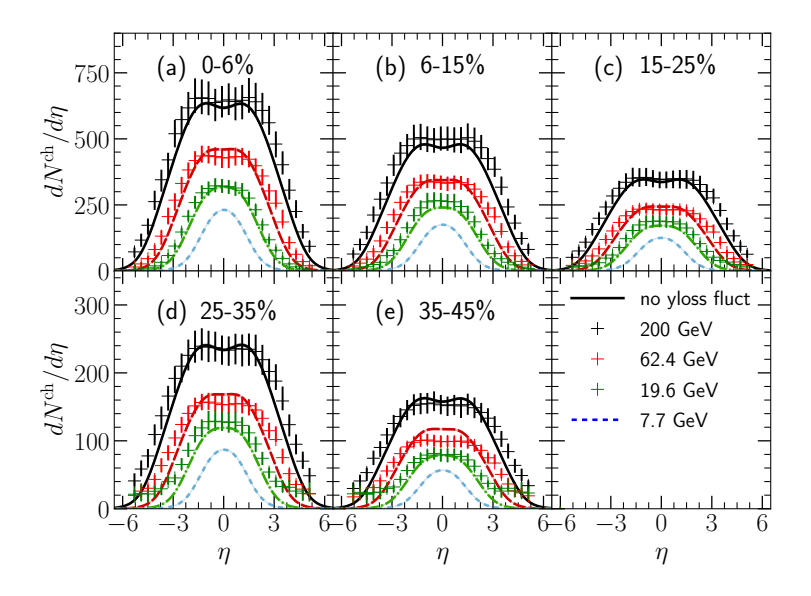
Coupling the new dynamic initial state to the hydrodynamic simulation MUSIC via sources as described above and in [261], which in turn is coupled to UrQMD, which performs hadronic rescattering, we can obtain an all particle spectra differential in rapidity and transverse momentum.

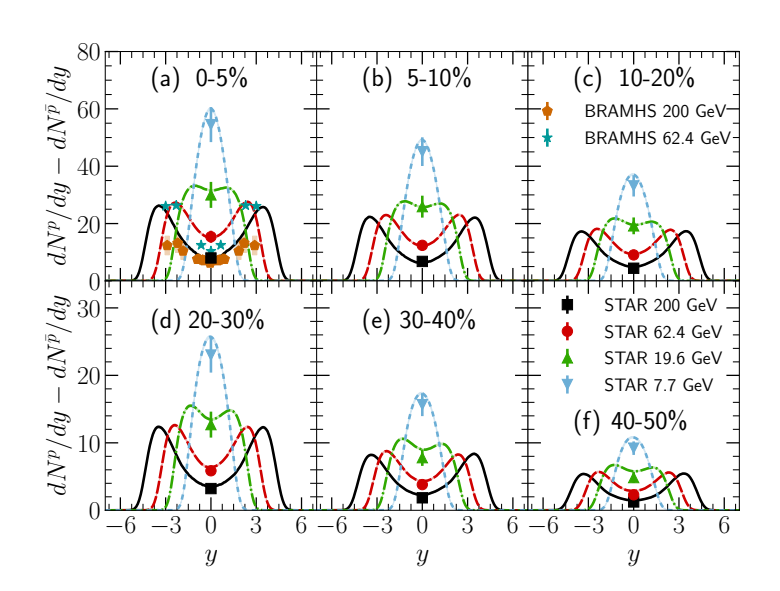
In Fig. 14 we present results for transverse momentum integrated charged hadron rapidity distributions at various collision energies in di erent centrality classes in Au+Au collisions and compare to experimental data from the PHOBOS Collaboration [257]. The centrality



and energy dependence is well described, yet most distributions are narrower than the experimental data. A ne tuning of the parameters and study of the e ect of uctuations in the rapidity loss of the decelerating quarks is still ongoing and could potentially lead to an improvement of the description of the experimental data.

In Fig. 15, we show net-proton rapidity distributions for different centrality classes and different collision energies in Au+Au collisions, and compare to experimental data from the BRAHMS [259] and STAR [258, 260] Collaborations. Except for most central events and the highest collision energies, experimental data are only available at midrapidity. Yet, the energy and centrality dependence of net-proton production is also well described, with the rapidity dependence in the 0-5% bin for 200 and 62.4 GeV collisions also agreeing rather well with the data. Unfortunately, rapidity distributions for net protons are not available for all





collision energies and centralities.

It is absolutely essential to describe the baryon stopping as realistically as possible when the goal is the extraction of critical uctuations from net-proton cumulants. Thus, the proper description of the average net-proton production over a wide range of energies and centralities is a necessary condition for a model to ful ll. More constraints on the model, particularly the baryon transport, can be obtained by comparing to experimental data from asymmetric systems, in particular d+Au collisions, for which data are available at di erent collision energies.

Prior to the BEST Collaboration, the collision energy dependence of radial and elliptic ow in heavy-ion collisions was investigated using boost-invariant simulations [265, 266]. At intermediate collision energies, the heavy-ion collisions break the assumption of longitudinal boost-invariance. Such non-trivial longitudinal dynamics was rst studied in a simplified 1+1D simulation [267]. Later, the rst 3D hydrodynamic + hadronic transport simulations with the UrQMD transport-based initial conditions found that the elective specific shear viscosity increases as collision energy is lowered [230].

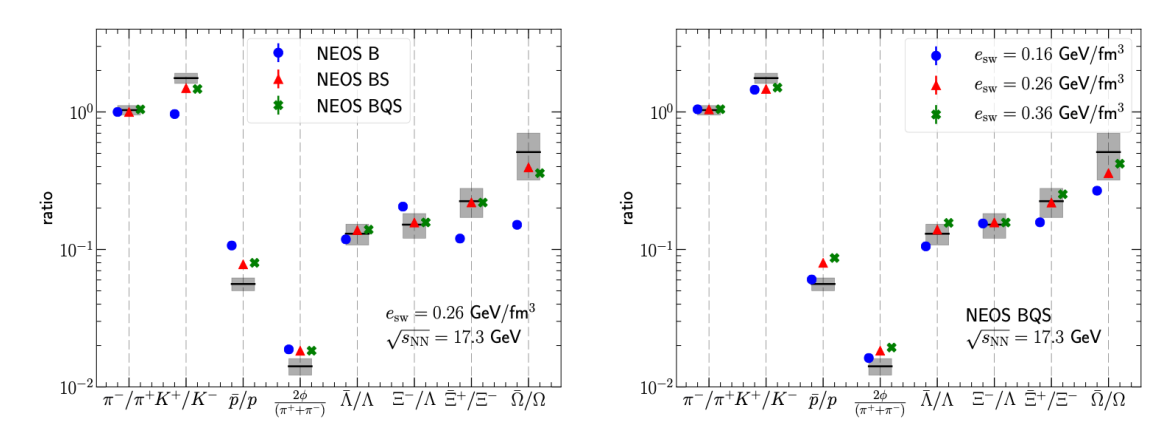
The viscous hydrodynamic treatment of heavy ion collision, which has been successfully applied to top RHIC and LHC energies, requires several essential extensions in order to be applicable for the energies relevant for the BES. At the lower energies the net-baryon density does not vanish and thus the theoretical framework needs to be able to propagate all the conserved currents, baryon number, strangeness, and electric charge. At low collision energies $\mathcal{O}(10)$ GeV, the nite longitudinal extension of the colliding nuclei has to be taken into account, which leads to a substantial overlapping time 1 3 fm/c during which the two nuclei pass through each other. The pre-equilibrium dynamics during this overlapping time may play an important role in understanding baryon stopping and density uctuations along the longitudinal direction of collisions. In order to quantitatively model the dynamics of heavy-ion collision at the RHIC Beam energy scan energies, the following ingredients are essential:

- Pre-equilibrium dynamics during the stage when the two colliding nuclei pass through each other.
- An equation of state at nite baryon density based on lattice QCD calculations, combined with a critical point controlled by a set of adjustable parameters.

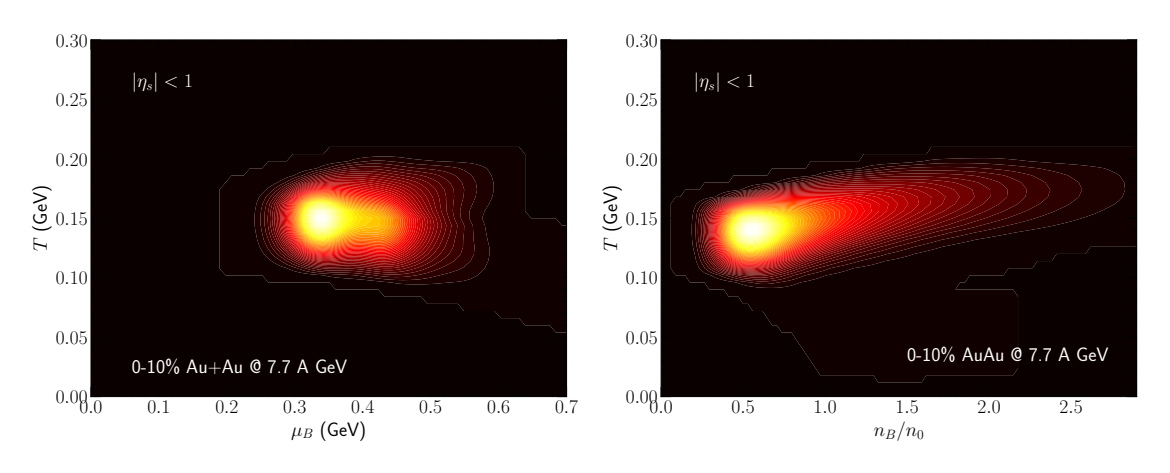
• Fluid dynamic equations for all conserved charges, including dissipative e ects.

We will describe progress on these issues below. For general reviews of hydrodynamic modeling at RHIC and LHC, and for de nitions of hydrodynamic observables we refer the reader to Ref. [5, 220, 268, 269].

Solving the equations of motion of hydrodynamics at intermediate and low collision energies requires an equation of state (EoS), which describes the thermodynamic properties of nuclear matter at nite baryon density. Current lattice QCD techniques cannot directly compute such an EoS because of the sign problem [49]. However, at vanishing net baryon density, or = 0, higher-order susceptibilities have been computed by lattice QCD [12]. These susceptibility coe cients were used to construct a nuclear matter EoS at nite baryon densities through a Taylor expansion [62, 63, 85, 270]. These EoS are reliable within the region where 2 in the phase diagram as shown in Sec. II A.

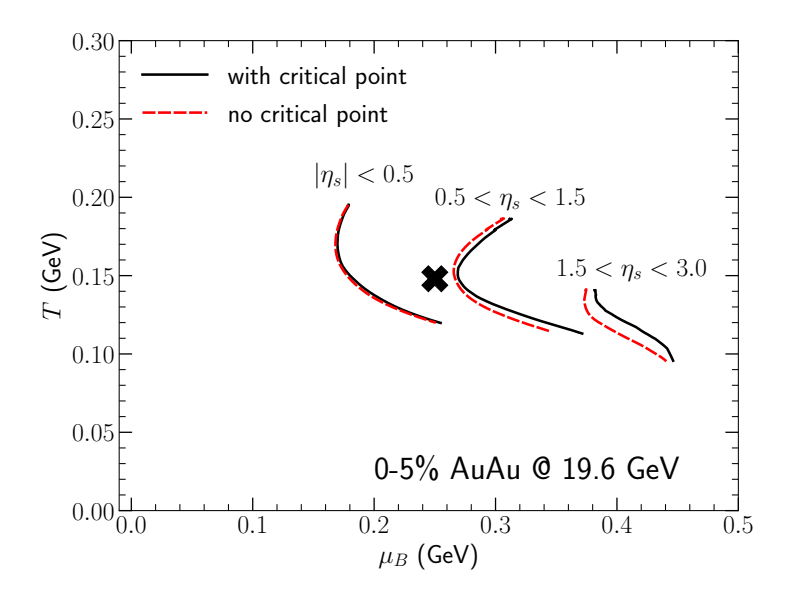


Let us now discuss the phenomenological impacts of various model ingredients, such as strangeness neutrality and presence of a critical point. Because the colliding nuclei do not carry any net strangeness, the strangeness density in nuclear collisions vanishes on average, = 0. This condition leads to 3 in the QGP phase [270, 272 274]. Fig. 16 shows the e ect of the strangeness neutrality on identi ed particle yields at 17.3 GeV. The relative yields of multi-strangeness baryons increase and agree well with the NA49 measurements once the strangeness neutrality condition is imposed. Further imposing = 0.4 introduces a small di erence between the and yields. The right panel shows the dependence of relative particle yields on the choice of switching energy density, at which uid cells are mapped to individual hadrons. A lower switching energy density yields smaller ratio of anti-baryons to baryons. A switching energy density 0.2 GeV/fm is preferred by the NA49 measurements at the top SPS collision energy.

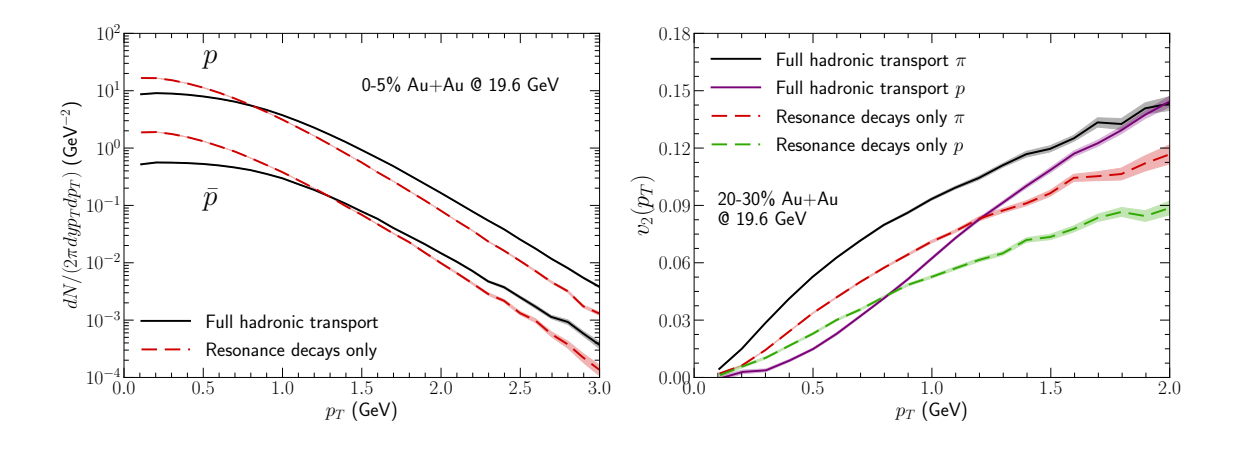


Once the dynamical simulations are calibrated with the particle production measurements, they can provide a realistic and detailed space-time evolution of the relativistic heavy-ion collisions. Fig. 17 shows the trajectories of an averaged 0-10% Au+Au collision at = 7 7 GeV in the QCD phase diagrams. These trajectories were analyzed from the hybrid simulations performed in Ref. [255], which was calibrated to reproduce the measured net proton yield at midrapidity. The 3D dynamical framework allows us to map individual heavy-ion collisions to the QCD phase diagram. At = 7 7 GeV, in the central rapidity region = 1, most of the reball explores regions with = [0 1 0 2] GeV and [0 25 0 5] GeV. The right panel shows the phase diagram as a function of the ratio of local net baryon density to the normal nuclear saturation density = 0 17

 $(1/\mathrm{fm})$. At 7.7 GeV collision energy, the majority of the uid cells in the reball reach about half of the nuclear saturation density, $0.1\,\mathrm{fm}$. During the early time of the evolution, the value of net baryon density can reach up to 0.5 fm , about three times normal nuclear density.



In Fig. 18, we explore the e ects of the presence of a critical point in the equation of state [85] on the averaged reball trajectories. The critical point and the line of rst-order phase transitions emerging from it for distort the adiabatic (=const) expansion trajectories [85, 275, 276]. We consider a critical point at = 148 MeV and MeV and study how it in uences the time evolution and the nal state observables of a heavy-ion collisions at 19.6 GeV. Fig. 18 shows that the reball trajectories shift to slightly values compared to whose from the simulations without the critical point. This e ect is consistent with the e ect of critical point on constant trajectories shown in Ref. [85]. The e ect is larger at forward rapidities, where the reball crosses the rstorder phase transition. The two phases are connected by a Maxwell construction [85]. This means that we are not trying to simulate nucleation or spinodal decomposition. Because the reball trajectories are averaged over a distribution of values from individual uid cells, the trajectory discontinuities at phase transition boundary are smeared. We nd that the two EoS with and without critical point result in very similar nal particle spectra and ow observables, indicating that these observables have limited sensitivity to the existence and location of a critical point. But note that the implementation of a rst-order phase transition at large — into the dynamical simulations has been somewhat rudimentary so far and requires further study.

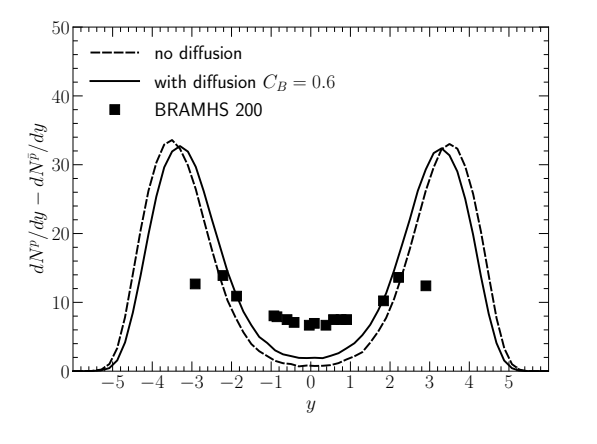


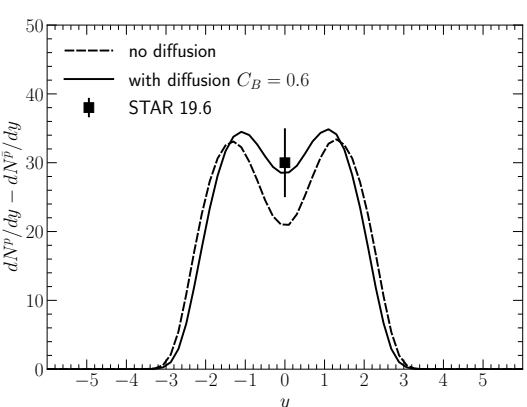
As the collision energy decreases, the hadronic dynamics becomes more and more important in describing the dynamics of relativistic heavy-ion collisions. Fig. 19 demonstrates the e ects of hadronic scattering on the shape of -spectra and () of identi ed particles at — = 19 6 GeV. Hadronic interactions atten both proton and anti-proton spectra because of scatterings with fast moving pions, known as the pion wind. The baryon rich environment at 19.6 GeV also results in a more prominent annihilation of anti-protons compared to what is observed at 200 GeV [63, 278]. The right panel shows that the elliptic ow coe cients of pions and protons continue to increase in the hadronic phase. The remaining spatial eccentricity continues to generate momentum anisotropy of particles in the hadronic transport phase, increasing the elliptic ow of pions and protons at high. The low protons—receives a blue shift from the—pion wind—, which increases the splitting between pion and proton—during the hadronic evolution.

At intermediate collision energies, the non-vanishing net baryon density forms a conserved particle number current in the hydrodynamic evolution,

$$= 0 \quad \text{with} \quad = \quad + \tag{14}$$

Similar to the energy-momentum tensor, the evolution of net baryon current involves dissipative e ects, controlled by the net baryon di usion current. Note that in the presence of a conserved baryon charge there are di erent frames that can be used to de ne the uid velocity. In the Landau frame the uid velocity is de ned by the condition that =, so that there is no dissipative contribution to the energy ux. The baryon di usion current—then characterizes baryon di usion relative to the energy current. In the Navier-Stokes limit, this di usion current—is proportional to local gradients of the ratio of net baryon chemical potential over temperature, (-B), where—is the baryon di usion constant [277, 279].

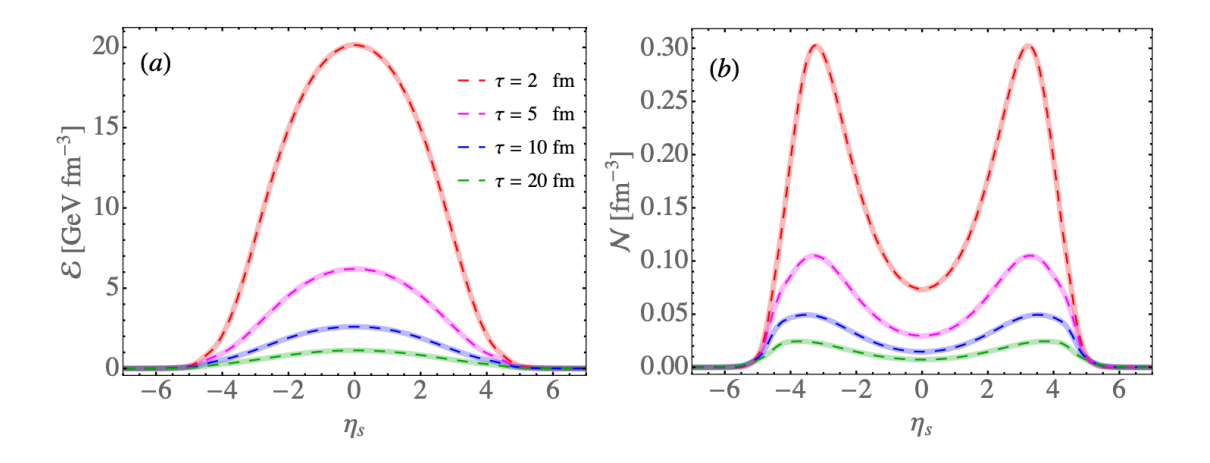




The e ects of net baryon di usion on phenomenological observables were systematically studied in Ref. [120, 277]. The —di erential observables for proton and anti-protons show strong sensitivity to the out-of-equilibrium corrections at particlization. Fig. 20 highlights the most prominent e ect of baryon di usion currents, which is a change in the rapidity distribution of net protons in heavy-ion collisions. A non-zero di usion constant —, proportional to the parameter — in Fig. 20, causes a shift of net baryon number from forward

rapidities to the mid-rapidity region. However, the e ect of baryon di usion during the hydrodynamic evolution alone is not enough to transport enough baryon charges to mid-rapidity in Au+Au collisions at 200 GeV. Therefore, the BRAMHS measurements suggested that there must be substantial baryon stopping during the early pre-equilibrium evolution of the relativistic heavy-ion collisions at 200 GeV. To extract the net baryon di usion coefcient from the experimental measurements, we need to disentangle the initial state baryon stopping from the baryon di usion during the hydrodynamic phase. Additional experimental observables, such as the charge balance functions, may help us to set a better constraint on unknown QGP transport coefficient in a baryon rich environment.

Relativistic hydrodynamic simulations in full (3+1)D require developing large-scale numerical code packages. It is essential to have open-source code packages and standardized benchmark tests among di erent implementations.



Within the BEST Collaboration, we performed numerical code validation among two independent implementations of (3+1)D hydrodynamic simulations with the propagation of net baryon current and its di usion. Fig. 21 highlights such a code validation between MUSIC and BEShydro for the propagation of net baryon current with di usion in a sim-

pli ed 1+1D longitudinal expansion [280]. The two numerical code packages independently implemented the equations of motion for hydrodynamic elds. The results agree with each other very well. A variety of additional code validation protocols for (3+1)-dimensional dissipative hydrodynamic codes are described in [280].

Before the establishment of the BEST Collaboration, the CME and CMW signals in heavy-ion collisions have been investigated using ideal chiral hydrodynamics [281, 282] which evolves non-dissipative chiral currents on top a of viscous hydrodynamic background [283, 284]. A next step towards a more self-consistent treatment of anomalous transport must take into account the non-equilibrium correction to both the bulk background and the vector and axial vector currents. This is achieved by the Anomalous-Viscous Fluid Dynamics (AVFD) simulation package [173, 210] which solves the evolution of vector and axial current, including dissipation e ect, as linear perturbation on top of the viscous hydrodynamic background.

In heavy-ion collision experiments, the CME-induced charge separation is measured by the charge-sensitive two-particle correlators, known as — and —. They are de ned as

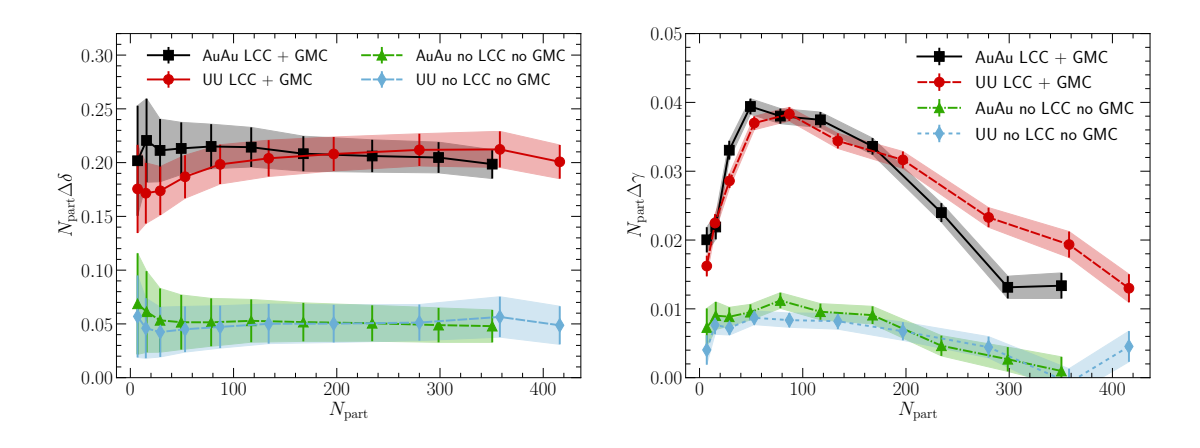
$$\cos(\quad + \qquad 2 \qquad) \tag{15}$$

$$\cos($$
) (16)

where is the reaction plane of the collisions. The indices and label the electric charge, = . To highlight the CME signal, experimentalists further consider the di erence between opposite-sign and same-sign correlators, (+) 2 and similarly for . Such correlators measure the uctuation of the charge separation vector, and contain not only the CME signal, but also the non-CME background. The major sources of such non-CME background come from the e ect of Global Momentum Conservation (GMC) and Local Charge Conservation (LCC). The GMC and LCC e ects imply non-vanishing multi-particle correlations, which makes it non-trivial to implement these e ects in the numerical simulation of freeze-out process.

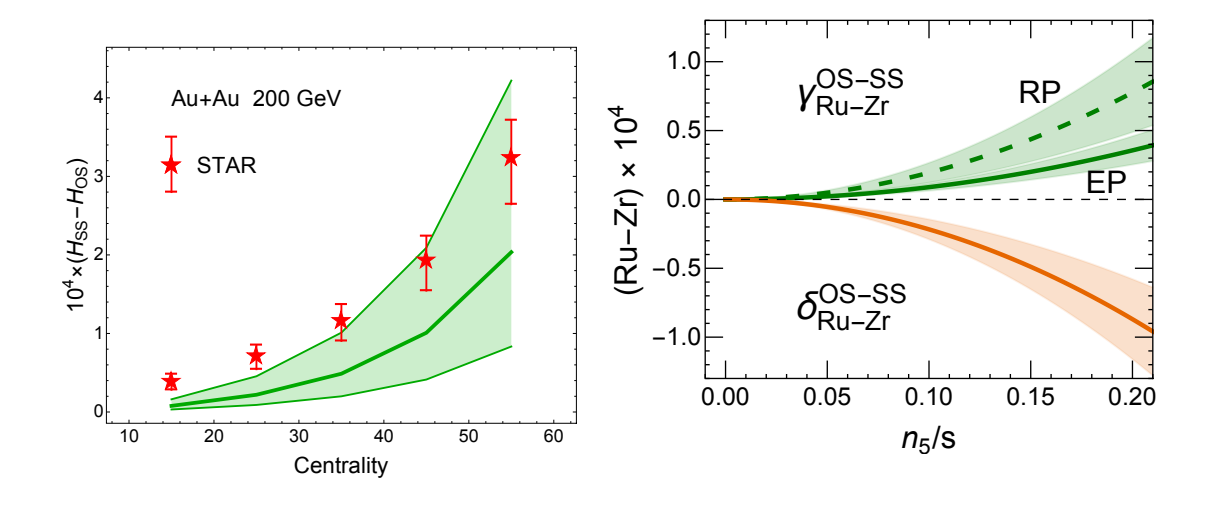
In [285], both the GMC and LCC e ects are implemented in the freeze-out process using the numerical implementation—rst proposed in [286]. In this work charged hadron-

antihadron pairs are chosen to be produced in the same uid cell, while their momenta are sampled independently in the local rest frame of the uid cell. This procedure implicitly assumes the correlation length to be smaller than the size of the cell, hence it provides an upper limit for the correlations between opposite sign pairs. In addition, the GMC is imposed by adjusting the momentum of nal state hadrons. As shown in Fig. 22, the LCC correlators, compared to the case with only resonance decay. e ect increases the and Meanwhile, GMC changes the absolute value of same-sign and opposite-sign correlators, but has negligible in uence on the di erence between them. Since then a more sophisticated prescription of particlization was developed by the BEST Collaboration [287, 288], which allows for a more realistic estimate of GMC and LCC e ects on the and correlators. As discussed in detail in Sec. VIII, this new particlization method employs the Markov Chain Monte-Carlo algorithm to sample hadrons according to the desired distribution, respecting the conservation of energy, momentum, baryon number, electric charge, and strangeness, within a localized patch of uid cells on the freeze-out surface.



Over the years the AVFD package has been further improved in essentially three stages: 1) in the rst generation [173, 210], the simulations start with event-averaged initial condition, and tested the sensitivity of the strength of CME charge separation with respect to a series of ingredients, particularly the axial charge imbalance and the magnetic eld lifetime. By

using reasonable parameters, the magnitude and centrality dependence of possible CME signal can be described, see Fig. 23 (left). 2) later, a second generation simulation [209] was developed, which takes into account the uctuating initial condition for hydro and magnetic eld, and implements the LCC e ect with prescription of Ref. [285]. As shown in Fig. 23 (right), a di erence of CME signals between the isobaric system is predicted, which can be tested in the on-going isobar experiment at RHIC. 3) in a continuing e ort of the BEST Collaboration, the AVFD package is upgraded to its third generation, and implements the micro-canonical particle sampler [287, 288], followed by the updated hadron transport simulation package, SMASH [289]. It provides a global description of CME observables for di erent collision systems, including both the CME signal and the non-CME background.



It is worth mentioning that two additional improvements are needed for a more accurate description of the CME signal. First, the evolution of non-conserved axial charge requires a more careful modeling, to take into account the thermal—uctuations and damping e—ects. The second is the time evolution of the electromagnetic—eld. Current versions of the AVFD calculation use a toy-model parameterization for the time revolution, and requires the input

from a more realistic MagnetoHydroDynamics (MHD) calculation. While the dynamical axial charge in under development in an on-going project by the BEST Collaboration, the current status of the dynamical electromagnetic field solver will be discussed in the rest of this subsections.

2. Evolution of Electromagnetic Field

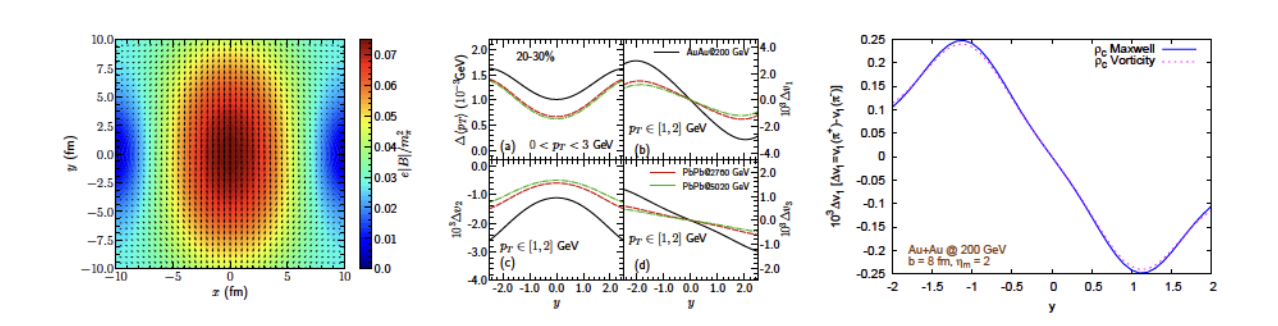


FIG. 24. (Left, reproduced from [180] with permission): The magnetic field in the transverse plane at z=0 in the lab frame at a proper time $\tau=1$ fm/c after a Pb+Pb collision with 20-30% centrality and with a collision energy $\sqrt{s_{NN}}=2.76$ TeV. (middle, reproduced from [180] with permission) The collision energy dependence of the electromagnetically induced charge-odd contributions to flow observables. The difference of particle mean p_T and v_n between π^+ and π^- are plotted as a function of particle rapidity for collisions at the top RHIC energy of 200 GeV and at two LHC collision energies. (right, reproduced from [179] with permission) Directed flow v_1 versus rapidity y, with an initial energy density distribution non tilted and tilted by using different values of the parameter η_m .

Significant efforts have been made within the BEST Collaboration to numerically solve the magnetohydrodynamic equations. In [180], the space-time evolution of the electromagnetic field is solved on top of realistic hydrodynamic evolution. This involves an analytical solution derived in [291] which assumes a constant, temperature-independent electric conductivity. The magnetic field profile at $\tau = 1$ fm/c in the 20-30% Pb+Pb collisions is shown in Fig. 24 (left). The EM induced modification of particle distribution, i.e. the difference of particle mean p_T and v_n between π^+ and π^- , are studied as shown in Fig. 24 (middle). In particular, a charge-odd directed flow, Δv_1 , and a triangular flow, Δv_3 , are found to be odd in rapidity. These effects are induced by the magnetic field via the Faraday effect and the Lorentz force,

as well as by the Coulomb eld of the charged spectators. In addition, the electric eld generated by the QGP with non-vanishing net charge drives rapidity-odd radial ow and elliptic ow . These studies assume that the evolution of the EM eld decouples from the hydrodynamic background, neglecting the feedback on the medium.

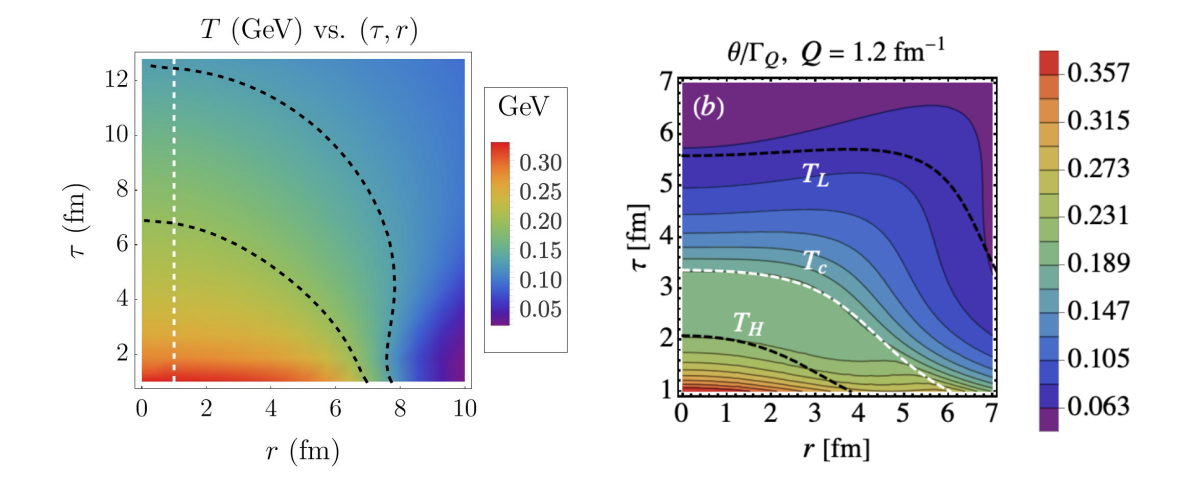
On the other hand, a study based on ideal magnetohydrodynamics was performed in Ref. [179]. The approach is based on solving the evolution of the bulk medium together with the EM eld, but it assumes in nite electric conductivity. The study nds similar behavior to the aforementioned electromagnetic eld induced modi cations, e.g. the chargedependent direct ow as shown in Fig. 24 (right). In both studies, the rapidity slope of are found to be opposite to the ALICE results [292]. Such tension rejects the delicate interplay between the Faraday e ect and the Lorentz force, which contribute oppositely to , and calls for a more realistic study of the evolution of electromagnetic eld. the sign of Moreover, a recent study [293] demonstrated we can the averaged transverse momentum of the collision system as an experimental handle to manipulate the magnitude of magnetic elds generated by the spectators. A new project by the BEST Collaboration, aimed towards a more realistic description of the space-time pro le of the magnetic eld in heavy-ion collisions, is in progress. The goal of this project is to solve the Maxwell equations together with the conservation equation of the electric current, taking into account realistic temperature dependent conductivities as perturbations to the hot medium. Similar to [180], the feedback to the medium is neglected and these equations are solved as perturbations.

As discussed in Sec. III there are two practical approaches for studying the dynamical evolution of critical uctuations near a QCD critical point: the deterministic approach, which solves a relaxation equation for the correlation functions, and the stochastic approach, which describes the same physics using stochastic equations similar to the Langevin equation. The study of critical dynamics in uids has a long history [294, 295], but until recently many important ingredients were missing in studies of critical dynamics in heavy ion collisions:

i The e ects of conservation laws (such as charge conservation) were missing. Since the order parameter relevant for the QCD critical point is associated with baryon density, charge conservation needs be treated properly for quantitative studies.

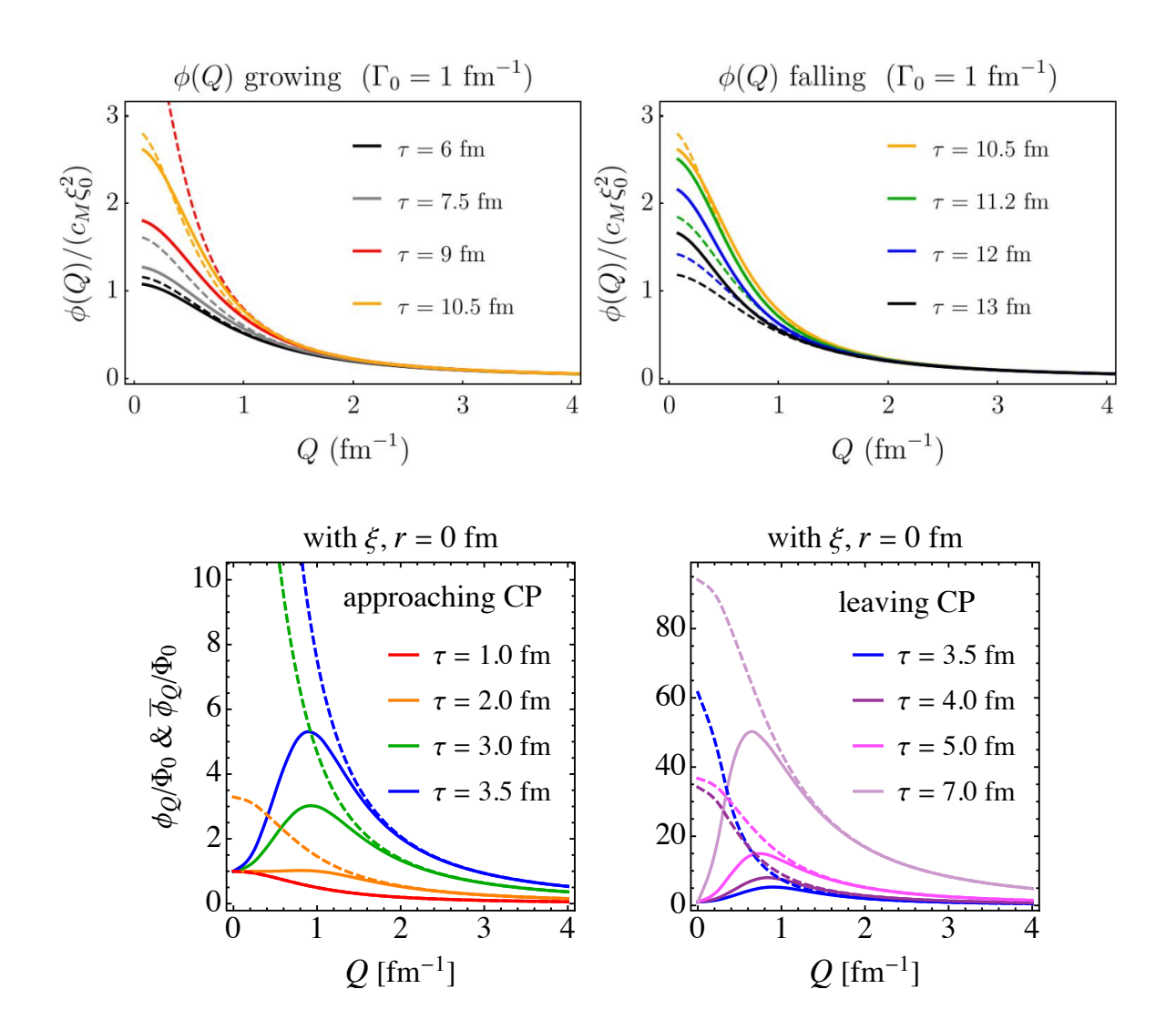
- ii Most studies considered a homogeneous and boost-invariant reball. Such a set-up is far from realistic and does not take into account the e ects of advection.
- iii While the qualitative importance of such out-of-equilibrium e ects has been well-appreciated, its quantitative relevance has not been fully studied.

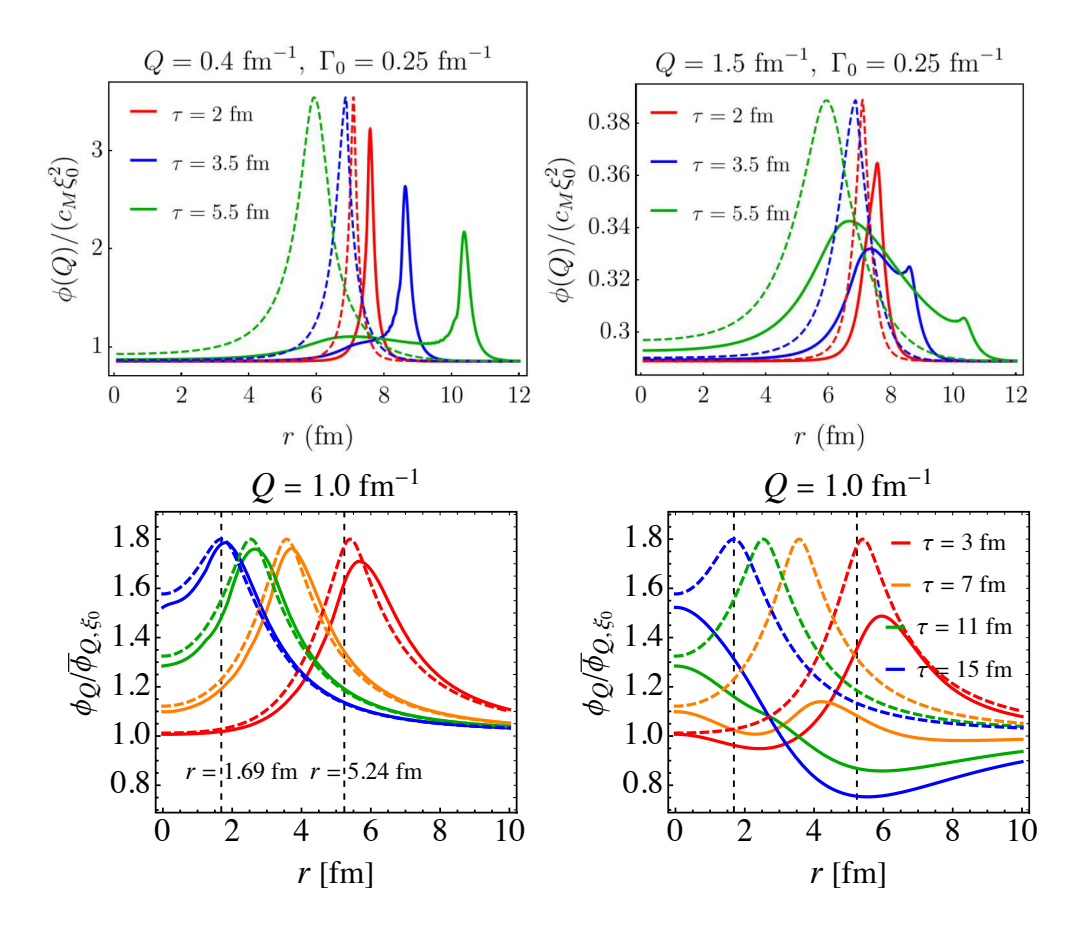
In the following, we shall strategy rest summarize the simulation results from Hydro+, which employs the deterministic approach, and discuss the progress towards addressing the aforementioned issues. At the end of this subsection we will summarize the progress and current status of stochastic hydrodynamics simulations.



There are two recent simulations within the Hydro+ framework, published in Refs. [117] and [118]. (See Sec. III A for a brief discussion of the ideas underlying Hydro+.) The goal of Ref. [117] was to explore Hydro+ in a minimal model. This model captures the interplay of critical uctuations and hydrodynamics in a setting where the dynamics is similar to that is encountered in a heavy ion collision while the geometry and equation of state are simplified. Specifically, Ref. [117] considers a radially and longitudinally expanding uid, which is boost-invariant and azimuthally symmetric in the transverse plane, and expands

along the temperature axis at = 0, with a hypothetical critical point located at small . In the exploratory study of Ref. [118], the authors follow the evolution of the two-point function of baryon density () (or) on top of a simpli ed QCD matter background, known as Gubser ow [296, 297]], with large non-zero baryon number. This set-up allows the authors to clearly distinguish the main e ects controlling the dynamics of long-wavelength uctuations and to explore systems with large baryon chemical potential. In Fig. 25, we plot the temperature pro les in the () plane for both studies.





We now discuss the main lessons learned in those simulations. First, both simulations demonstrate the need for describing the out-of-equilibrium evolution of uctuations quantitatively. Fig. 26 (upper panel) plots the temporal evolution of () (as a function of the momentum) from Ref [117] at = 1 fm, deep within the interior of the reball. We observe that, as expected, large modes stay in equilibrium. Hence we shall focus on small , i.e. long-wavelength modes from now on. We see that the temporal evolution of () at long wavelengths falls out of equilibrium in two characteristic stages. First, at earlier times as () rises as the cooling QGP approaches from above, () lags behind Fig. 26 (upper left panel). At later times, as () drops as the QGP cools away from toward lower temperature Fig. 26 (upper right panel) () shows a memory e ect: the dashed curve remembers where the dashed curve used to be (Fig. 26, upper panel, right). The phenomena of lag and memory are also apparent in Fig. 26 (lower panel) where we plot the

results from Ref. [118] at = 0 fm. Qualitatively, the behavior at small [117] and large [118]] is similar, but the —dependence of the transport coe—cients leads to signi—cant quantitative di—erences if (as suggested by lattice QCD and BES experiments) the critical point is located at large—. To summarize, (—) encodes information about the criticality, which is why we are working towards describing it quantitatively.

As a second lesson we learn that conservation laws play an important role in dynamics. This can be seen by comparing the behavior of () at a small in the two studies. Ref. [117] and Ref. [118] implement the dynamical universality class of model A (for a non-conserved order parameter) and model B (for a conserved order parameter), in the classication of Hohenberg and Halperin [295]. The relaxation rate () approaches a constant for the former and vanishes as for the latter. We observe that a conserved order parameter () at small stays at its initial value. This clearly demonstrates the crucial role of the conservation law: (= 0) corresponds to the uctuation of the order parameter averaged over the whole volume. If the order parameter is associated with conserved densities, then the uctuation at = 0 can not evolve at all.

The third lesson is that radial ow transports uctuations by advection, and that quantitative studies are required to understand this e ect. To see this, let us rst look at Fig. 27 (upper panel) where we show vs at the representative value of = 0.4 fm from [117]. We observe that the peak in equilibrium expectation of () moves inward as a function of time. On the other hand, the spatial dependence of the fully dynamical () is determined by the combination of two out-of-equilibrium e ects. First, the memory and lag e ects imply that as the peak in the equilibrium curve (dashed) moves inward, the actual at its location increases toward it but does not come close to reaching it. Second, the peak in the uctuations is carried outward by advection in the expanding uid. To further illustrative those two e ects, let us look at Fig. 27 (lower panel) where we show vs from Ref. [118]. In Fig. 27 (lower panel, left), the advection term in Hydro+ equation is switched on (lower right panel), signi cant changes in the evolution of the -dependence of are observed.

A fourth lesson is that the non-equilibrium contributions due to slow modes to bulk properties such as entropy and pressure are generally small. In [117] the authors found tiny back-reaction corrections to the background evolution. This is further con rmed in Ref. [118]. Speci cally, the out-of-equilibrium slow-mode contribution to the entropy

density is of the order

$$-- \mathcal{O}(10 \quad 10 \quad) \tag{17}$$

This can be understood by comparing the phase space volume of out-of-equilibrium critical modes (2) with the typical entropy density:

$$-- \frac{1}{(2)}(--) --$$
 (18)

where denotes the typical momentum which is not in equilibrium. Using the value = (4 (1) + 21), which corresponds to the entropy density of an ideal QGP at zero baryon chemical potential, we arrive at () $\mathcal{O}(10)$.

This conclusion is consistent with a study of the critical behavior the bulk viscosity near the QCD critical point [298]. Bulk viscosity controls the non-equilibrium contribution to the pressure in an expanding uid. In a near-critical uid, the dominant e ect arises from the lag in the order parameter relative to its equilibrium value. The critical bulk viscosity is of the form

$$(19)$$

where is constant of proportionality, and is the correlation length away from the critical point. Ref. [298] found that is quite small, 10 on the crossover side of the transition, although it is very sensitive to the mapping between the QCD EoS and Ising EoS. Based on the estimate in [90], we also expect 2. Finally, we note that bulk viscosity itself also exhibits critical slowing down, and the nonequilibrium contribution to the pressure is smaller in magnitude than the equilibrium expectation = .

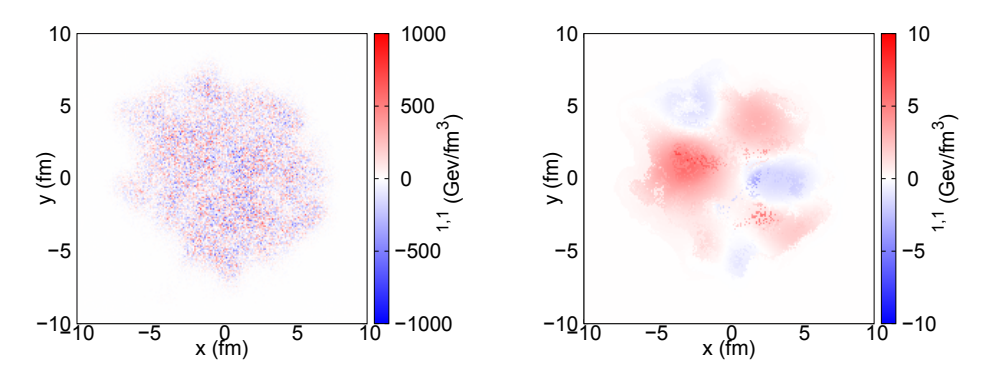
From a practical perspective, the smallness of back-reaction e ects suggests one may neglect the back-reaction in future phenomenological modeling, which will signicantly reduce computational cost.

A di erent method to include stochastic e ects in hydrodynamics and to consider the thermal uctuations that are demanded by the uctuation-dissipation theorem is to generalize the energy-momentum tensor, , by including a noise term. Explicitly, to the usual ideal and viscous parts, a random uctuating term is added:

$$= + + + \qquad (20)$$

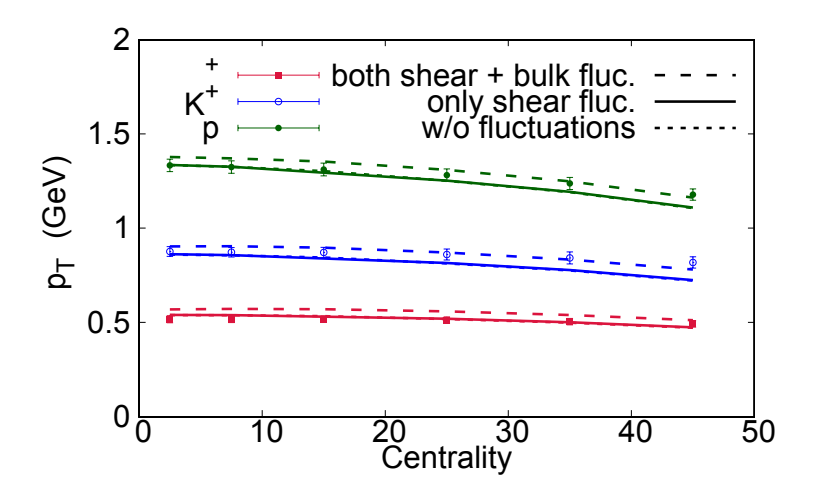
The introduction of the noise term leads to a feature absent from treatments without thermal uctuations. The autocorrelation of noise is proportional to a delta function:

where and are the shear and bulk viscosity coe cients, = , and and are space-time four vectors [97, 108]. The introduction of thermal uctuations turns the hydrodynamical evolution into a stochastic process where the noise is sampled over the space of a uid cell, at each step in proper time [299]. However, the averaged noise will diverge with decreasing cell size. This indicates that the theory needs to be renormalized. In the perturbative approximation—where the uctuation is separated from the uid dynamical background—equations for the noise and its response decouple from the hydro evolution equations [300]. An approach which goes beyond the perturbative limit is discussed next.



Hydrodynamics is a macroscopic, long wavelength theory. One notes that the $\,$ nite cell size can suppress all wavelengths below 2, where $\,$ (). The discrete grid acts as a low-pass $\,$ lter allowing only modes with wave number less than $\,$. Consider, as an example, uctuations of shear modes. On physical grounds, one can argue that shear modes with a wave number larger than $\,$ 1 () will quickly relax to equilibrium. Here, $\,$ is the decay time for the dissipative stresses to relax to the Navier-Stokes form, and $\,$ = $\,$ (). These fast modes are in thermal equilibrium, and their contribution to physical observables is accounted for in the equilibrium equation of state and the transport coe-cients.

In typical simulations the cuto scale set by the inverse cell size is much larger than the physical scale set by the relaxation time. In practical applications it makes sense to remove the fast modes with wave numbers greater than 1 () by an additional low pass lter, see also [303 305]. In [304], the dependence of the hydrodynamical elds and their uctuations on the lattice spacing is demonstrated. In the following we will use the kinetic theory relation to write , where is a parameter of order 1. A procedure to implement a local low pass lter in relativistic uid dynamics is described in Ref. [301]. It is based on boosting uid cells to the local rest frame, Fourier transforming, imposing a wave number cuto, and then performing the inverse transformation. The local coarsegraining limits both noise and ordinary gradients that have the potential to invalidate the second-order uid dynamical treatment. The e ect of noise ltering is illustrated in Figure 28, which displays an element of the noise tensor, for a collision of Pb + Pb at TeV, in a 0 5% centrality class, at mid-rapidity, before and after the noise- ltering process [302].



We leave the details to a forthcoming publication [307], but the thermal uctuations demanded by the uctuation-dissipation theorem do have e ects on observables that are

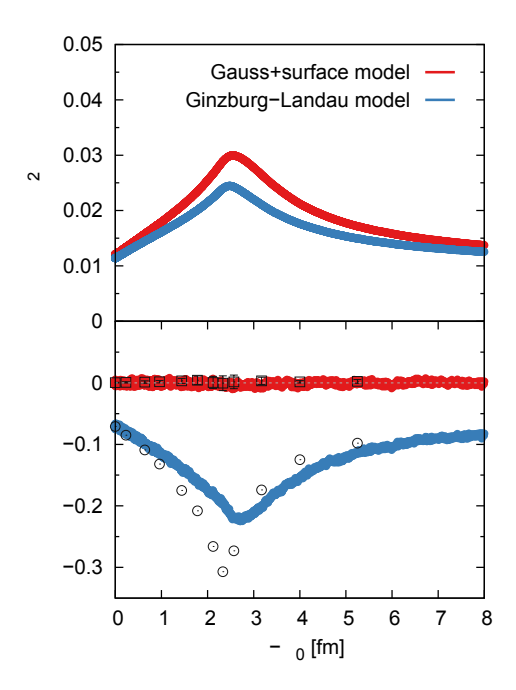
known to highlight the presence of uctuations, thermal or otherwise. The rst of those is the class of event-plane correlators, which are the correlations between the event planes generated by di erent harmonic coe cients [308, 309], and another are the linear and non-linear elements of the decomposition of the ow coe cients for higher harmonics (4), as prescribed in Ref. [310]:

$$=$$
 $+$ (22)

Importantly for the physics pursued by the BEST Collaboration, the inclusion of both shear and bulk dissipation modes do have an e ect on the phenomenological extraction of the transport coe cients of the hot and dense strongly interacting matter. In particular, the uctuations associated with the bulk viscosity a ect directly the net cooling and expansion of the reball, as seen in Fig. 29 which reports on calculation of the average transverse momentum for di erent charged species. The far-reaching conclusion of those studies is that the inclusion of thermal uctuations will entail the recalibration of transport coe cients in general, as observed in Fig. 29. A similar conclusion was also reached in Ref. [299], and it should impact the analysis of heavy-ion collisions at all energies, including those performed at the LHC, and the BES runs.

In what concerns the physics pursued here, the results obtained with stochastic hydrodynamics up to now applied to high-energy heavy-ion collisions need to be compared with simulation relying on the Hydro+ framework. The two approaches should be complementary, and their comparison will bene t the community as a whole. Then, the approach to criticality will be considered.

Returning to the physics of the critical point, the authors of Ref. [311, 312] consider uctuations of the net-baryon density near the critical point. They solve the stochastic di usion equation in a nite-size system with Gaussian white noise, using an Ising-like equation of state in 1+1 space-time dimensions. In contrast to earlier simulations of chiral uid dynamics (e.g. Ref. [99]), where the critical mode was identified with the non-conserved sigmal eld, the critical mode was taken to be a conserved density. The elects of charge conservation in a nite system modify the equilibrium scaling of the cumulants relative to the expected scaling with the correlation length in an in nite system. Typically, the critical growth is reduced, as explained in [313]. In the exploratory calculation described in [311, 312] the expected dynamical scaling behavior and the impact of critical slowing down are observed.



In particular, the results shown in Fig. 30 demonstrate that Gaussian noise, combined with a non-linear free energy functional, will generate the expected non-Gaussian cumulants, and that these cumulants show the e ects of memory and lag. Currently, the stochastic di usion equation is studied in expanding systems [314, 315] and in 3+1 dimensions, where ultraviolet divergencies related to the nite lattice spacing are more important, and renormalization of the equation of state and the transport coe cients has to be taken into account [316]. Higher-order cumulants have also been studied in the deterministic approach, see [114].

Proton number—uctuation cumulants are one of the primary experimental observables to probe the QCD critical point on the phase diagram [317, 318]. The critical point signal in the measurements of event-by-event—uctuations of protons should manifest itself in deviations of the corresponding measures from the baseline expectations that do not incorporate any critical point e ects. One simple choice for the baseline is a Poisson distribution, which would correspond to an uncorrelated proton production. However, the event-by-event—uctuations of protons in heavy-ion collisions, especially the high-order cumulants, are a ected by a number of non-critical mechanisms which make the non-critical reference distribution considerably more involved than that given by Poisson statistics.

The total net baryon number in heavy-ion collisions is determined by the colliding nuclei and conserved throughout the course of the collision. Baryon conservation thus introduces correlations between particles. For instance, any newly created baryon has to be counterbalanced by an anti-baryon elsewhere in the reball in order to ensure conservation of total baryon number. For this reason alone, cumulants of the proton number distribution will show deviations from Poisson statistics. One can argue that these corrections are small when one measures—uctuations in a small part of the whole system, as in this case the small acceptance ensures the applicability of the grand-canonical ensemble [319]. However, the e ects of baryon conservation become large in high-order proton number cumulants that are used in the search for the QCD critical point, as—rst investigated in Ref. [320] in the framework of ideal gas of baryons and anti-baryons.

Recently, a subensemble acceptance method (SAM) was developed [321] that allows one to evaluate the e ect of global conservation on cumulants measured in a subsystem of the full system. To illustrate the e ect of global conservation, consider the ratio of baryon number cumulants — inside a subvolume of uniform thermal system that are a ected by

global baryon conservation. These are given by [321]

$$--- = (1 \qquad) --- \tag{23}$$

$$--=\begin{pmatrix} 1 & 2 \end{pmatrix} -- \tag{24}$$

$$-- = \begin{pmatrix} 1 & 3 & \end{pmatrix} -- 3 & -- \tag{25}$$

Here is a fraction of the total volume covered by the subvolume, = 1, and are the grand-canonical baryon number susceptibilities. These expressions demonstrate that the e ect of baryon conservation disappears in the limit = 0, but that at small = 0 nite the deviations are larger for higher-order cumulants.

More recently, the SAM has been extended to the case of multiple conserved charges [322], as well as non-uniform systems, non-conserved quantities (like proton numbers), and momentum space acceptances [323]. The formalism can be used to either subtract the e ect of global conservation of multiple charges from experimental data, or to include the e ect in theoretical calculations of proton number cumulants.

Another source of particle correlations may come from short-range repulsive interactions between hadrons, commonly modeled through the excluded volume [324]. The presence of the excluded volume corrections suppresses the variance of particle number—uctuations [325]. In particular, the HRG model with excluded volume e—ects in the baryon sector leads to an improved description of lattice QCD susceptibilities at temperatures close to the chemical freeze-out in heavy-ion collisions [326–328]. As the excluded volume corresponds to purely repulsive interactions, it does not induce criticality, thus it is a source of non-critical—uctuations. Incorporating the excluded volume e—ect in heavy-ion collisions is challenging and requires modi cations to the standard Cooper-Frye particlization. Progress in this direction has recently been achieved, either through a Monte Carlo sampling of an interacting hadron resonance gas at particlization [329], or an analytic calculation of the proton number cumulants [80].

Event-by-event uctuations of the system volume, which are linked to the centrality selection and cannot be avoided completely in heavy-ion collisions, comprise an additional source of proton number—uctuations [330, 331]. The volume—uctuations generally lead to an enhanced variance of—uctuations, whereas their e ect on the high-order proton cumulants depends on the corresponding cumulants of the volume distribution. The volume—uctuations can also be regarded as a manifestation of event-by-event—uctuations in the initial state. It is important to incorporate this e—ect in theoretical calculations to match the relevant experimental conditions. In some cases, the e—ect of volume—uctuations can be removed (or minimized) from the experimental data, making the theoretical interpretation of the data easier [332].

An appropriate non-critical baseline for proton number uctuations can be obtained within a dynamical description of heavy-ion collisions which incorporates the essential noncritical contributions. While some non-critical e ects, like baryon conservation, can be analyzed without dynamical modeling [333], modeling is necessary to treat all the dierent e ects simultaneously. This has recently been achieved in the work [80] in the framework of (3+1)D relativistic hydrodynamics applied to 0-5% central Au-Au collision at RHIC-BES energies. The simulations utilize collision geometry based 3D initial conditions [255] and viscous hydrodynamics evolution with a crossover-type equation of state NEOS-BQS [63] and simulation parameters adjusted to reproduce bulk observables. The Cooper-Frye particlization takes place at a constant energy density of = 0.26 GeV/fm, where the cumulants of the (anti)proton number are calculated in a given momentum acceptance analytically. The calculations take into account both the repulsive interactions and global baryon conservation. The former are incorporated in the framework of the excluded volume HRG model, in line with the behavior of baryon number susceptibilities observed in lattice QCD [328]. The e ects of global baryon number conservation are taken into account using a generalized subensemble acceptance method [323].

Figure 31 shows the collision energy dependence of the net proton cumulant ratios

 $\kappa_3/\kappa_1 \equiv S\sigma^3/M$ and $\kappa_4/\kappa_2 \equiv \kappa\sigma^2$ in comparison with the experimental data of the STAR Collaboration [75]. These ratios are equal to unity in the Skellam distribution limit of uncorrelated (anti)proton production. Both baryon conservation and excluded volume lead to a suppression of these two ratios, which monotonically increase with collision energy. The stronger effect of baryon conservation at low energies can be explained by larger fraction of particles ending up at midrapidity compared to higher energies, while the enhancement of baryon repulsion is due to larger baryon densities achieved at lower $\sqrt{s_{\rm NN}}$. It is also clear that baryon conservation has a larger influence at all energies compared to the excluded volume. However, both effects are necessary to obtain a quantitative description of the $S\sigma^3/M$ data at $\sqrt{s_{\rm NN}} \geq 20$ GeV. At lower energies the data indicate a smaller suppression of $S\sigma^3/M$ than predicted by the calculation. As for the $\kappa\sigma^2$, the STAR data show possible indications for a non-monotonic collision energy dependence which is not observed in the baseline calculation, however, more precise data at the lowest energies are required to make a robust conclusion.

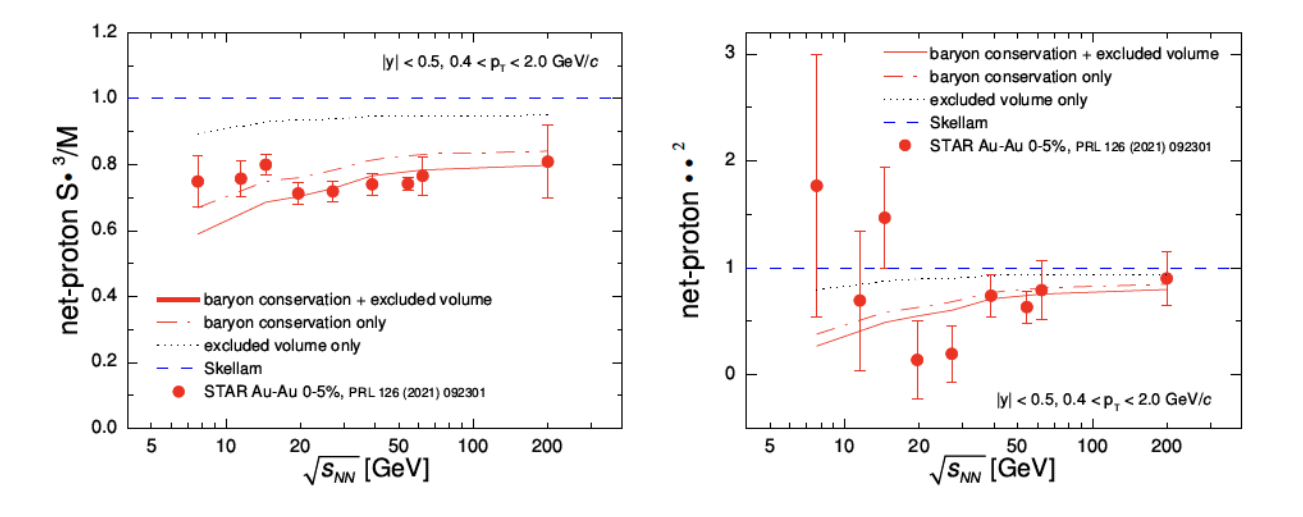


FIG. 31. Collision energy dependence of the net-proton cumulant ratios $\kappa_3/\kappa_1 \equiv S\sigma^3/M$ (left) and $\kappa_4/\kappa_2 \equiv \kappa\sigma^2$ (right) in 0-5% Au-Au collisions at RHIC BES energies in a non-critical scenario compared with the STAR measurements [75, 80]. Calculations use The (3+1)D hydrodynamic medium calibrated in Ref. [255] and impose exact global net baryon conservation and excluded volume corrections. The figure is adapted from Ref. [80].

Additional insights can be gained by analyzing proton and antiproton distributions separately. In particular, one can study, in addition to the ordinary cumulants, the (anti)proton

correlation functions (factorial cumulants) , which probe genuine multi-particle correlations and thus should be sensitive probes of the critical behavior. Figure 32 shows the collision energy dependence of the scaled factorial cumulants , , and of protons and antiprotons. The second factorial cumulants of both the protons and antiprotons indicate negative two-particle correlations. The results for protons agree with the experimental data at ______ 20 GeV but overestimate the strength of negative correlations at lower collision energies. The data for antiprotons are reproduced qualitatively, however, in contrast to the protons, here the calculation underestimates the negative two-particle correlations in the collision energy range 19.6 GeV _______ 62.4 GeV.

The high-order factorial cumulants, and , exhibit a behavior which is quite di erent from the corresponding ordinary cumulants. The calculations indicate the presence of only mild multi-particle correlations among protons in the non-critical scenario. The baryon conservation and excluded volume e ects lead to small positive , which agrees with the available experimental data. For the four-particle correlations one obtains

1. This also agrees with the available experimental data within error bars, although the errors in the data are large for _____ 20 GeV. If future measurements establish sizable multi-proton correlations, then this result would be discult to describe in a non-critical scenario.

The goal of this section is to provide an overview over advances made by the BEST Collaboration in the area of particlization and kinetic transport in the hadronic phase, in particular:

- Microcanonical particlization
- Particlization of hydro+
- Hadronic transport with adjustable mean- eld potentials

Dynamical models of heavy-ion collisions typically involve both a hydrodynamic stage and a hadronic transport stage. Hydrodynamic description applies in systems that are largely

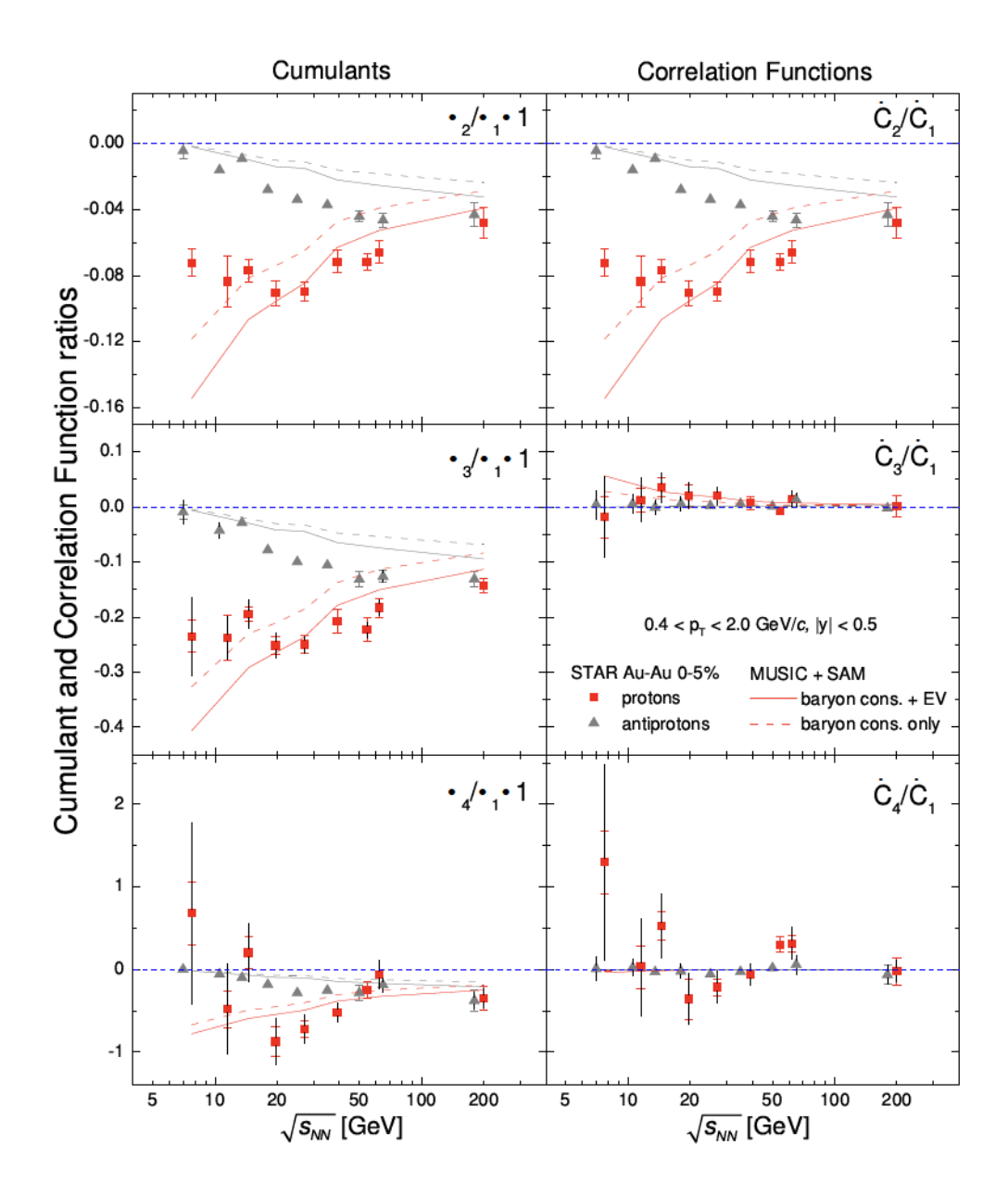


FIG. 32. The scaled proton and antiproton cumulants and factorial cumulants (correlation functions) in 0-5% Au+Au collisions at RHIC BES energies in a non-critical scenario compared with the STAR measurements [80, 334]. Calculations use The (3+1)D hydrodynamic medium calibrated in Ref. [255] and impose exact global net baryon conservation and excluded volume corrections. The figure is adapted from Ref. [80].

equilibrated. However, as the system expands, the matter cools and hadronizes. Once hadrons form, it becomes increasingly difficult to maintain local equilibrium. A hadron gas consists of hundreds of species with masses ranging from 135 MeV/ c^2 to a few GeV/ c^2 . As the matter cools and becomes more dilute, inelastic collisions are too rare to maintain

chemical equilibrium, and chemical equilibration times are much longer than the lifetime of the hadronic stage [335, 336]. Even local kinetic equilibrium is di cult to maintain, in part due to the wide range of masses. A gas of non-relativistic particles, with masses much larger than the temperature , cools such that 1 as the volume whereas massless particles cool as 1 . Thus, without a high collision rate heavy particles cool faster than light particles. Further, lighter particles, due to their higher thermal velocities, tend to di use through their heavier neighbors in a phenomenon known as the pion wind. Once the species no longer ow together, a hydrodynamic description is no longer appropriate [337]. This stage is most suitably described by molecular dynamics or Boltzmann approaches. In a molecular dynamics approach one samples representative particles, which collide and interact with one another by the experimentally known or modeled cross sections of hadrons in a dilute environment. Microscopic models of this type are sometimes referred to as afterburners. If one over-samples the particles by some factor and assigns each test particle a reduced charge of 1 while at the same time reducing the cross sections by the same factor, one arrives at a test particle representation of the Boltzmann limit.

Several physical observables are modi ed during the afterburner stage:

- Spectra and ow. Hadronic kinetics typically does not a ect pion and kaon yields as well as spectra by more than few percent. Proton yields can be changed by around 10% to 30%, depending on collision energy, mainly due to annihilations. Baryon spectra shift towards higher transverse momenta due to the pion wind e ect. Elliptic and radial ow are usually increased by an afterburner stage. These e ects are demonstrated in Fig. 19. Overall, the impact of the afterburner is significant, but at least some of the e ects can be taken into account by implementing partial chemical equilibrium in the hydrodynamic stage [338, 339]. Given the uncertainties of particlization and the afterburner itself (e.g. unknown cross sections, resonance properties, disculty or impossibility of implementing multi-particle reactions, uncertainties of in-medium interactions), this can be an escient approach at the higher energies, however, it has not been tested in the case of afterburners that include mean-eld escent.
- Fluctuations and correlations. The extent to which uctuations are a ected by hadronic kinetics is still being investigated. There are indications that di usion due to rescattering in the nal stage smears particle distributions and therefore changes uc-

tuation observables [340]. On the other hand, a direct check of net-charge, net-proton, and net-kaon correlations shows only minor afterburner e ects on these observables, despite con rming the presence of di usion and isospin randomization [341]. Overall, the role of the afterburner for uctuations and correlations requires further studies.

• The role of mean- eld potentials in hadronic transport in the energy range explored by the Beam Energy Scan is not well studied, because the inclusion of mean- eld potentials is computationally expensive, and additionally the potentials are not well constrained theoretically at high baryon densities. Mean- eld potentials change the equation of state in the low-temperature high-baryon-density region, where lattice QCD calculations at present cannot provide theoretical inputs. Using adjustable mean-eld potentials one can explore the sensitivity of observables to the equation of state in this region.

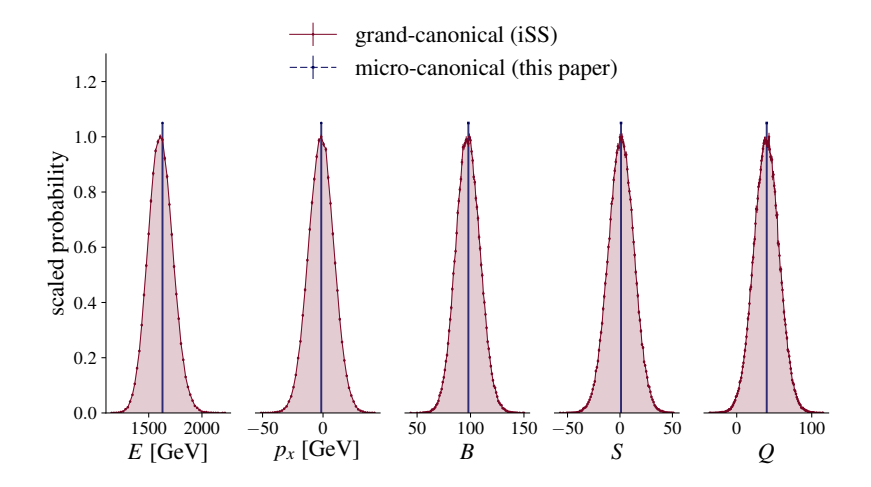
The interface between the hydrodynamic and microscopic stages is known as particlization. During this process the energy, momentum and charge carried by the uid is transformed into a distribution of particles, which on average reproduces the conserved quantities. Building such an interface requires confronting several issues. First, the hyper-surface that separates the hydrodynamic and microscopic domains, known as the particlization surface, moves relative to the uid. For most of the emission the particlization surface is spacelike, and there is no possibility for particles to re-enter the hydrodynamic domain from the hadronic stage. However, in some instances the particlization surface may be timelike, similarly as in the case of evaporation from a static surface, and then one must consider the e ect of trajectories reentering the hydrodynamic region, a phenomenon known as back ow [342]. Di erent algorithms handle back ow di erently. Another place where algorithms vary is in the implementation of viscous corrections. These variations can alter the values of especially at high . A third challenge facing the interface involves the implementation of local charge, energy, and momentum conservation. It is critical to account for such e ects when analyzing correlations and uctuations. Many of the hadrons generated at the inter-100 MeV. Because these widths are not much less face are resonances, with large widths than the temperature, accounting for the widths is also critical. Finally, the hadronic simulation might also incorporate mean elds. These can alter yields or masses, and the interface must be designed so that energy and momentum is preserved throughout the particlization process in such a way that the particle distributions are thermodynamically consistent.

Although many of the challenges listed above had been addressed prior to the e orts of the BEST Collaboration, additional progress was made in several areas. This includes the implementation of conservation laws and nite resonance widths at the hydrodynamic interface, and the implementation of mean elds. For this report we focus on three areas where the BEST contributions are particularly significant.

- Microcanonical particlization [287, 288]. We have developed a method that takes into account local conservation of charge and momentum in the particlization process, which is a crucial ingredient for a proper description of uctuation measurements.
- Particlization of Hydro+. We have shown how to imprint uctuations from Hydro+ onto produced hadrons. This allows us to quantify manifestations of critical behavior in nal-state measurements.
- Hadronic transport with adjustable potentials. Mean- eld potentials have previously been implemented at lower (e.g., GSI) energies, where the high baryon densities lead to large e ects. These e ects have been largely ignored at the highest RHIC energies or at the LHC. For BES energies, the e ects should again be important, but unlike at the lower energies one must account for hundreds of hadronic species.

In this section we rst brie y summarize recent progress in handling particlization in case uctuations and correlations are of interest. A local microcanonical approach is suitable for uctuating hydrodynamics, where uctuations are realized as uctuations in a set of hydrodynamical simulations. Another approach is required for particlization in hydro+, where second-order correlations and uctuations are available already at the hydrodynamic stage and need to be transferred correctly to particles. Then we proceed to discussing the hadronic afterburner with adjustable mean- eld potentials

Hydrodynamic approaches with stochastic terms produce an ensemble of events which encode the uctuations and correlations. For example, consider uctuations of baryon number in a certain rapidity and transverse momentum window. Suppose that there are



runs, and in each of them this baryon number is di erent. The distribution of includes both thermal and non-thermal (critical, initial state) uctuations. Therefore, the sampling should not introduce additional thermal uctuations, because they are already present in the ensemble of the hydro runs. For this one needs microcanonical sampling.

The concept of microcanonical sampling is shown in Fig. 33. In contrast to the usual grand-canonical sampling, where energy, net baryon number, net strangeness, electric charge are conserved on average over samples, in microcanonical sampling they are conserved in each sample. In [287] we have proposed a mathematical method for implementing microcanonical particlization and introduced the concept of patches—compact space-time regions on the particlization hypersurface, where conservation laws are enforced. Some methods to obtain the correct—xed energy, momentum, and charges in every sample were suggested previously, see [343] for overview. However, none of these earlier approaches produces the correct microcanonical distribution in the simple limiting case of microcanonical sampling in a static, uniform box. In the follow-up work [288] we have tested our method in a realistic setup and explored some e ects of the microcanonical sampling on heavy-ion observables. The main conclusions of the work are the following:

• The decomposition of the hypersurface into patches on which the conservation laws are

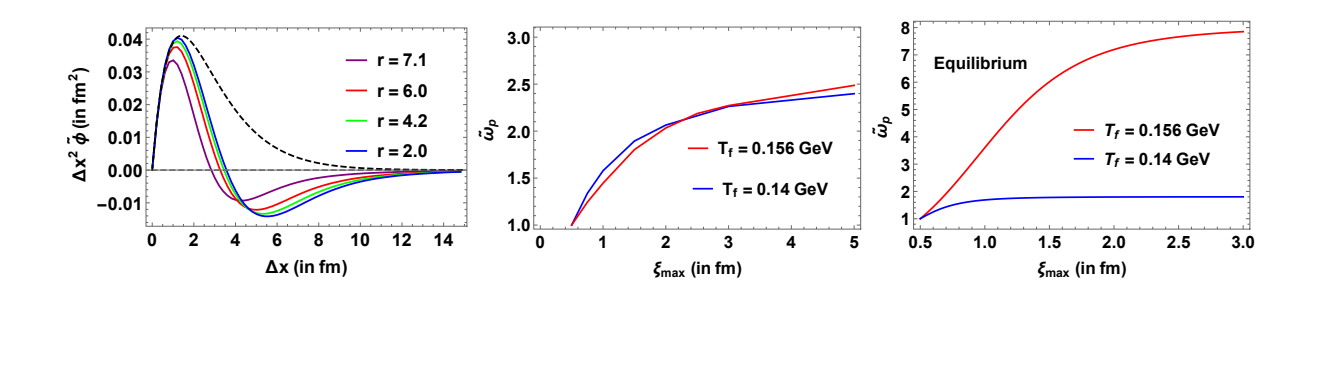
enforced can be controlled by a parameter—the rest frame energy of the patch in our case. Even after this parameter is—xed, there is a considerable freedom in selecting the location of patches. However, the e ect of this additional freedom on observables is significantly smaller than the e ect of the patch energy parameter. This allows for meaningful applications of our method.

• Fluctuations and correlations are signi-cantly a ected by event-by-event conservation laws. Mean values, such as spectra and ow, are only a ected in small systems, or in the limit of small patches.

We have integrated our open-source microcanonical sampler into a framework with the SMASH hadronic afterburner and found that the e ects of microcanonical sampler on uctuations and correlations survive until the end of the afterburner evolution [288]. This means that if one studies correlations and uctuations with an afterburner, then a microcanonical sampler is required for consistency.

The input data for particlization in Hydro+ is di erent from that in stochastic even-by-event hydrodynamics. In stochastic hydrodynamics correlations and uctuations are embedded in an ensemble of hydrodynamic events. In contrast, Hydro+ simulations directly provide the mean and the two-point correlation functions of the hydrodynamic densities near the critical point. In this section we show how particle correlations and uctuations can be computed in this case, and we present some initial results, see Ref. [344]. These results illustrate how to translate correlations on a Hydro+ freeze-out hypersurface into predictions for experimental observables such as particle multiplicities and their cumulants. Ref. [344] proposes a freeze-out procedure to convert the critical uctuations in the hydrodynamic stage into cumulants of particle multiplicities. The idea is to introduce a critical sigma eld, so that uctuations of the eld are imprinted on the observed hadrons due to the coupling of the sigma eld to hadrons.

As explained in the previous section, the traditional Cooper-Frye procedure [345] matches only the averages of the conserved densities between the hydrodynamic and particle descriptions on the freeze-out hypersurface. This is inadequate near a critical point. To ensure



that the two-point correlation functions describing the critical uctuations are carried over to the particle description, one needs to employ an extended freeze-out prescription near the critical point.

The critical uctuations are incorporated in the kinetic (particle) description via an e ective coupling between the particles and the critical sigma eld, , which modi es the masses of the particles. The modi ed particle distribution function is given by:

Here, denotes the particle species and () is the particle distribution function without including the critical e ects, which is taken to be the Boltzmann distribution function. The coupling measures the strength of the interaction between the particles of species and the sigma eld. In the preliminary study only pions, nucleons and their anti-particles were included, but the model can be extended to a full hadron resonance gas in a straightforward manner. The eld is a stochastic variable such that:

$$() = 0 \qquad () () = () \qquad -() -() \qquad (27)$$

where is an appropriately chosen normalization factor. The two-point correlation function of the entropy per baryon, denoted as , is obtained from Hydro+ simulations, for example those of Ref. [117]. The resulting modi cation to the particle masses changes the variance of the particle multiplicity distributions,

$$=$$
 () ' () () () (28)

Here, and ' are di erential elements on the freeze-out hypersurface pointing along the direction of the normal at and respectively. in Eq. (28) is given by:

$$=2 \qquad \frac{}{(2)} \qquad (29)$$

The result in Eq. (28) gives an estimate of critical e ects in the variance of the particle multiplicity. As an exploratory study, this procedure is used to freeze out the system generated in a Hydro+ simulation obeying Model H relaxation dynamics in an azimuthally symmetric boost invariant background (see Sec. III A). The ratio of the variance de ned in Eq. (28) to the mean multiplicity is denoted as ,

$$= ----$$
 (30)

The excess of the critical uctuations over the non-critical baseline can be quanti ed, via de ned below

$$=$$
 — (31)

where is the estimate for when the correlation length is microscopic and equal to some non-critical value. obtained within the Hydro+ framework for the simulation from Ref. [117] is shown in Fig. 34.

This procedure can be extended to higher moments and employed to calculate higher cumulants of particle multiplicity once higher order—uctuations from hydrodynamic simulations are available. This work has the potential to quantitatively addresses the e ects of critical slowing down and conservation laws on particle number cumulants, assuming that these observables are not substantially modi ed by the hadronic transport stage. These modi cations could be studied by generating an ensemble of—eld con—gurations satisfying Eq. (27), and then propagating particles through the kinetic regime.

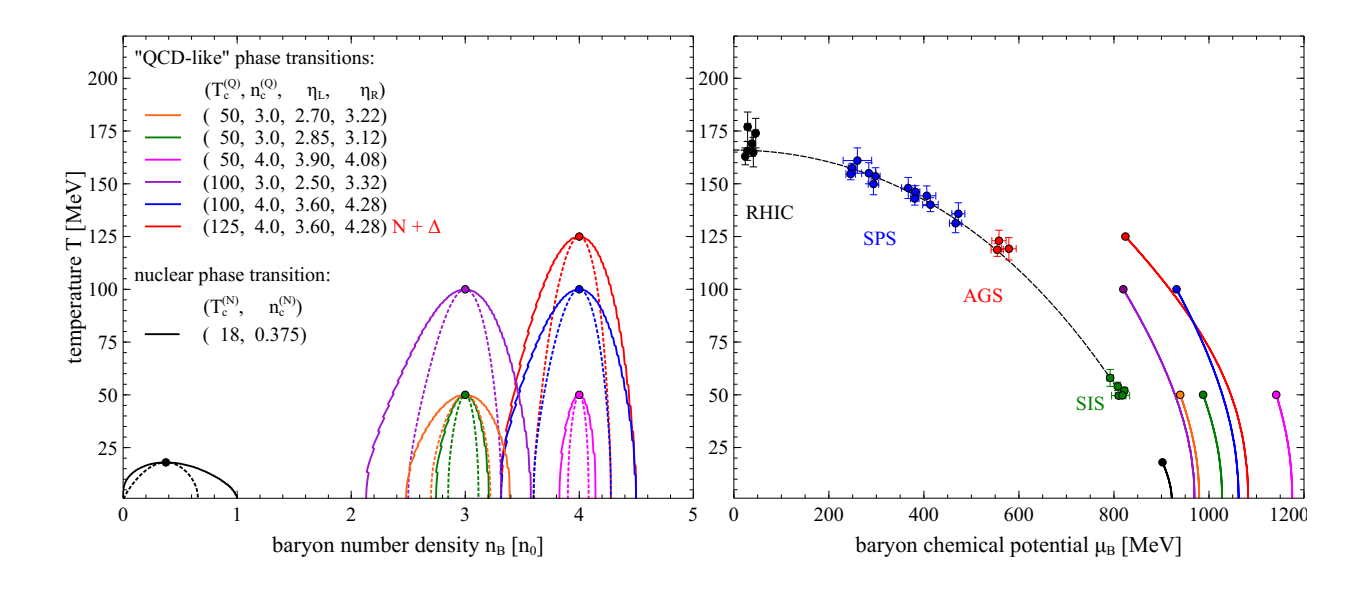
Lattice QCD calculations of the equation of state of nuclear matter at nite baryon density can only reach chemical potentials—up to about 400 MeV and temperatures down to around 120 MeV, which corresponds to maximum baryon densities around—. For higher baryon density and lower temperature, an ideal hadron resonance gas equation of state is often assumed in the simulations. However, in this (vast!) region of the phase diagram there is a nuclear liquid-gas phase transition, and the possible—rst-order QCD phase transition between hadrons and the quark-gluon plasma. An afterburner with adjustable mean—eld potentials can provide a versatile equation of state in this region and allows studies of the following questions:

- What region of () or () can one probe, in principle, through heavy-ion collisions? Note that while some regions might be reached in practice, there might be no observable sensitive enough to signal such an occurrence.
- How sensitive are the observables to the equation of state in the high-density region? How much do the nuclear liquid-gas and the possible QCD phase transitions in uence observables at RHIC BES energies?

Besides these questions, adjustable potentials are useful to smoothly match the equation of state used in hydrodynamics to the one realized in kinetic transport.

Despite these features, afterburners are often run in the cascade mode, in which meaneld interactions between hadrons are neglected. Although this is done in large part to achieve better numerical e-ciency, another reason for doing so is the fact that the meaneld potentials commonly used in hadronic transport are only—t to reproduce the behavior of cold nuclear matter, and as such do not contain information on the possible in uence of the QGP phase transition on the nuclear matter EOS. However, this means that the role of many-body interactions in the hadronic stage of a heavy-ion collision evolution is largely unexplored, and it is possible that transport simulations are missing important e-ects at high baryon densities, where both the mean-- elds and the time that the system spends in a hadronic state are substantial.

To address this issue, we developed a vector density functional (VDF) model of the nuclear matter equation of state (EOS) [346]. This functional can be easily parameterized to



reproduce a given set of the properties of a nuclear matter EOS, and at the same time it leads to relativistic single-particle dynamics that allows for a numerically estimated in a hadronic transport code.

For applications to heavy-ion collision simulations, we to the VDF EOS to describe hadronic matter with a phase diagram that contains two rst-order phase transitions. The rst transition is the experimentally observed low-temperature, low-density phase transition in nuclear matter, sometimes known as the nuclear liquid-gas transition. The second is a postulated high-temperature, high-density phase transition that is intended to correspond to the QCD phase transition. Because the degrees of freedom employed in the VDF model are baryons and not quarks and gluons, we will refer to the latter of the described phase transitions as a QGP-like phase transition.

In this variant of the VDF model the pressure takes a simple form

$$=$$
 $\frac{1}{(2)}$ $\ln 1 + \qquad ^{p} \qquad + \qquad \frac{1}{i}$ (32)

where $_{\mathbf{p}}$ is the quasiparticle energy and $_{\mathbf{p}}$ denotes the baryon number density. The corresponding single-particle equations of motion are

$$\underline{} = \underline{} \tag{33}$$

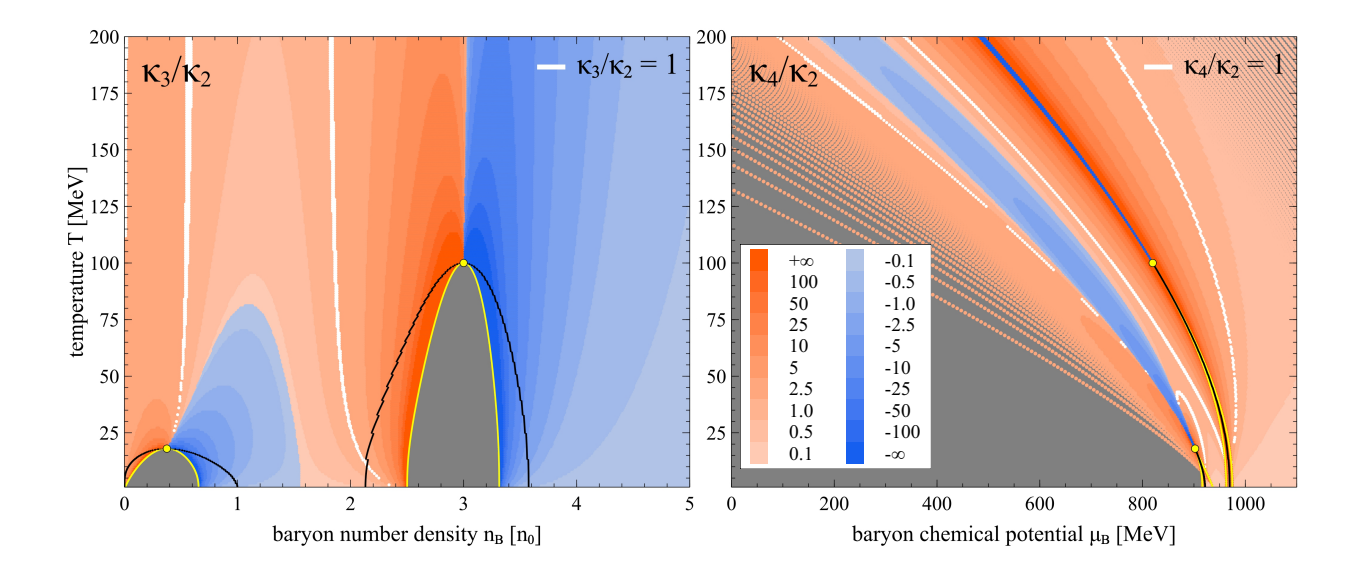
where is a vector eld associated with the baryon current,

$$(;)$$
 (35)

In the above formulae, are interaction parameters that are xed by requiring that the EOS reproduces the desired behavior of nuclear matter, including features of the phase transitions.

In Fig. 35 we show coexistence and spinodal region lines for several representative a QGP-like phase transitions, specified by the position of the QGP-like critical point and the boundaries the corresponding spinodal region. It is evident that the VDF model is able to produce an array of phase diagrams corresponding to different proposed properties of the QCD phase transition. In Fig. 36, we plot cumulant ratios in the fig. and figure planes, calculated using one of the representative EOSs. The behavior of the cumulant ratios, in particular their values exceeding or falling below the Poissonian limit of the phase transition, agrees with well-known expectations [216, 348].

The VDF equations of motion (33 and 34) have been implemented in the hadronic transport code SMASH [289]. We veri ed that the mean- eld hadronic transport reproduces the known properties of ordinary nuclear matter, such as the value of the binding energy at the saturation density, and the spinodal lines that characterize the unstable region of the nuclear phase transition. We show the evolution of the baryon number density for a system initialized inside the spinodal region of the proposed QGP-like phase transition in Fig. 37. In this gure, the red curve corresponds to the distribution at time = 0, while the blue curves delineate the distribution at times = 0. At = 0, the distribution is peaked at the initialization density = 3, but in the course of the evolution the system separates



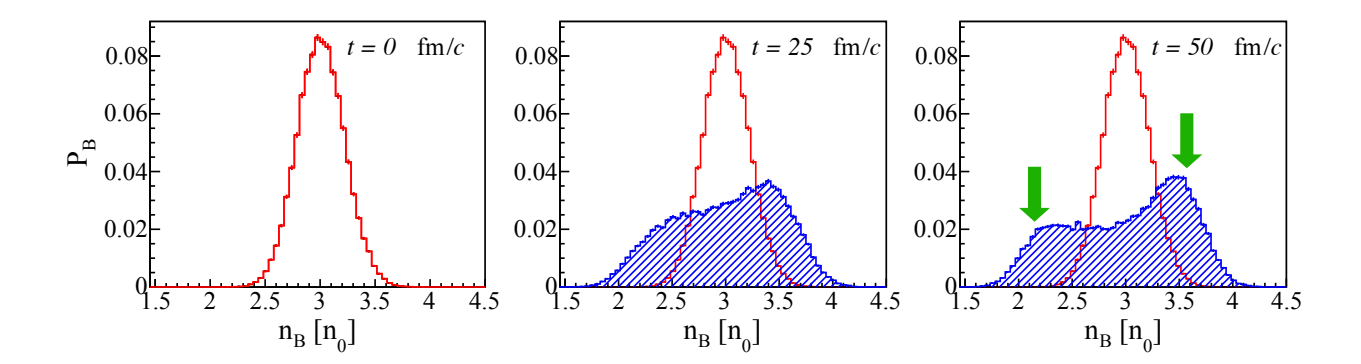
into two coexisting phases, a less dense and a more dense nuclear liquid. As a result, the nal distribution displays two peaks largely coinciding with the theoretical values of the coexistence region boundaries, =2.13 and =3.57; in the gure, these values are pointed to by green arrows.

Our exploratory studies show that mean- eld hadronic transport is sensitive to critical behavior in nuclear matter, and that this behavior is exactly what is expected based on the underlying theory. The correct description of both thermodynamics and non-equilibrium phenomena implies that hadronic transport can be used as a tool with unique capabilities to investigate the dynamic evolution of matter created in heavy-ion collisions.

The next step, currently in progress, is to employ these adjustable potentials in heavy-ion collisions and determine to what extent the QGP-like phase transition a ects observables. Preliminary ndings show that at $\overline{} = 7.7$ GeV these e ects are small. This is not surprising, given that in these collisions the system spends a very short time at densities above 2 , as one can see for example in Fig. 17. However, at the energies explored in xed

target experiments at RHIC, and at the HADES experiment at GSI [349], larger densities are explored and the QGP-like phase transition may have stronger e ects on observables. Whether the e ects due to a phase transition can be distinguished from the e ect of uncertain parameters in the model has to be studied carefully, for example by using the Bayesian analysis method.

The data from BES I and II runs are voluminous and heterogeneous. Measurements span a wide range of beam energies and centralities for a variety of beams. The experiments comprise numerous target and projectile combinations, and are analyzed by hundreds of collaborators within STAR and PHENIX. Theoretical models of heavy-ion collisions are similarly complex, as the nall observables depend on the three stages of the collision: pre-thermal evolution, hydrodynamic evolution and the nall decoupling stage. Each stage requires a different modeling paradigm. The decoupling stage is typically described by a microscopic

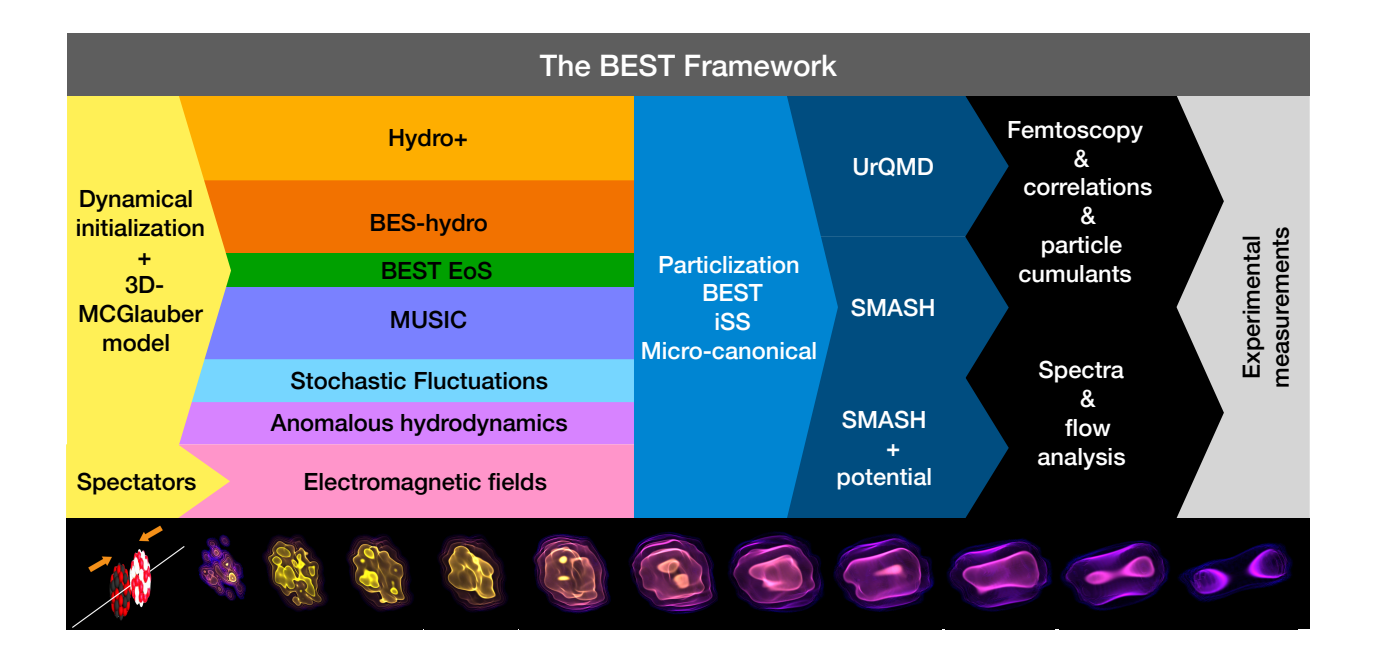


simulation using hadronic degrees of freedom, in contrast to the hydrodynamic degrees of freedom for the middle stage. The initial stage might be described by the evolution of classical elds, a microscopic simulation involving partons, or simply a parametric form. Thus, one needs to carefully design and test interfaces between each stage to faithfully model the behavior of the degrees of freedom.

The fundamental questions addressed by the RHIC program do not easily map onto speci c measurements that can be isolated and addressed with only a single type of observable. Instead, all observables (especially those related to soft physics) must be considered simultaneously. For example, changing the shear viscosity a ects the anisotropic ow coe cients, the mean transverse momentum, the multiplicity and femtoscopic correlations. The anisotropic ow coe cients are sensitive to the viscosity, the equation of state, and details of saturation and stopping in the pre-thermal stage.

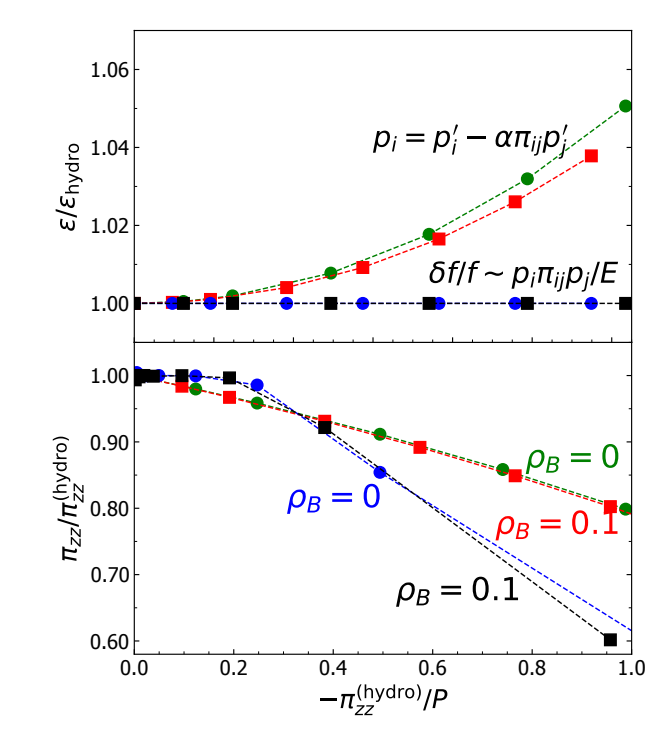
Global analyses of higher-energy data have now been performed for data from = 200 GeV RHIC collisions and from LHC collisions. By simultaneously addressing several classes of observables, these analyses are enabling rigorous scientic determination of fundamental quantities such as the viscosity or equation of state. At the highest energies, the hydrodynamic stage alone provides a major impact with respect to a ecting nal-state observables. For BES data, the system spends a larger fraction of its time in the nal-state hadronic stage and in the initial pre-thermal stage, thus increasing the importance of how these two stages are treated. Because of the larger non-uniformity in rapidity and the increased baryon density, the stopping and thermalization stage of low-energy collisions is inherently more discult to model and more rife with theoretical uncertainty. For these reasons, along with the fact that a larger range of beam energies is considered, a global BES analysis will be significantly more challenging, both numerically and theoretically, than the high-energy analyses.

The BEST Collaboration addresses the challenge laid out above in two ways. First, the BEST modeling infrastructure is modular and the individual components are being thoroughly tested. Secondly, the design will accommodate a global Bayesian analysis aimed at rigorous expression of fundamental parameters describing the bulk properties and evolution of high-density QCD matter. In the following section, we outline the structure and status of the BEST modeling framework, then describe how this will be applied to the interpretation of BES data.

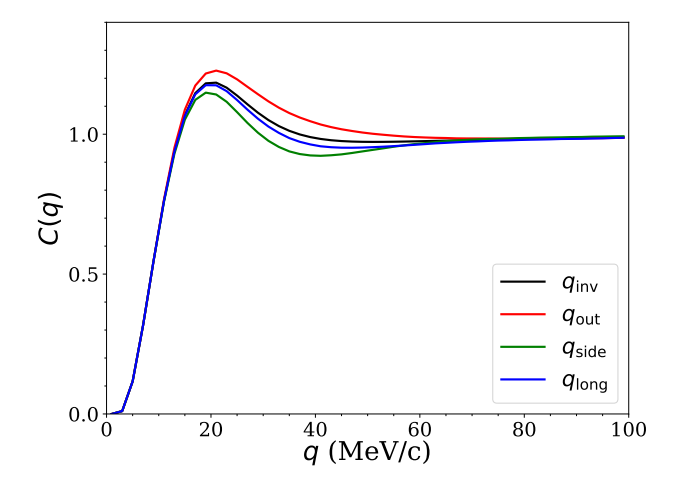


Modeling heavy ion collisions requires accurate descriptions of three phases, pre-thermal evolution, hydrodynamics, and a hadronic simulation describing the nal evolution and decoupling. Additionally, interfaces between di erent phases must be developed. Rigorous extraction of fundamental parameters requires a careful and thoughtful Bayesian comparison of experimental data to model output. The models used in such analysis must faithfully express the entire breadth of reasonable possibilities. This necessitates a modular design of the modeling framework, so that competing theoretical paradigms can be compared and distinguished. For that reason, the three principal modeling components are each designed as interchangeable modules with well de ned and carefully tested interfaces between modules. Figure 38 illustrates the design, emphasizing both the modularity and work ow.

The utilization of standard formats enables the plug-and-play functionality. For example, the nal-state particles resulting from the hadronic simulation are written in OSCAR format [350], which provides both the asymptotic momentum of each particle and its last point of interaction. From this information, the analysis code can construct single-particle observables like spectra and ow, two-particle femtoscopic correlations, and multiplicity uctuations. Hydrodynamic codes produce a list of hyper-surface elements in a standard



format from which the particlization codes produce a set of hadrons consistent with the stress-energy tensor at the interface between the hydrodynamic- and hadronic-simulations. The interfaces are exible by design. For example, Fig. 39 illustrates how accurately the viscous correction to the stress-energy tensor is reproduced by the sampled particles at the boundary between the hadronic simulation and the hydrodynamics description. The codes permit the user to choose between di erent representations of the viscous shear corrections to the phase space density.



_

The modeling framework produces lists of emitted hadrons. This includes the PID (particle identication code), momentum and the space-time coordinates of its last interaction. BEST software allows the user to quickly produce spectra and ow coecients. This will include composite particles, i.e. light nuclei [353]. Femtoscopic correlations, as illustrated in Fig. 40 are also readily generated. Analysis codes can also be easily exchanged and are unacted by choices of modules from earlier stages of the collision, as long as the observables consider nal-state hadrons emerging from the hadronic simulation. For particles emitted from earlier stages such as photons and dileptons, analysis codes can use hydrodynamic histories, but these formats might vary, or not even exist, for some modules.

Once the modeling infrastructure is complete, the BEST Collaboration will perform a global analysis of BES data, focusing on soft observables such as ow coe cients, spectra and femtoscopic source sizes. The procedure will follow that described in Refs. [33, 218, 223, 354 364]. Those analyses provide a sampling of the model parameters weighted by the posterior Bayesian likelihood. In previous analyses the number of model parameters, which we will collectively denote , have exceeded a dozen in some analyses. However, for a global BES

analysis the number of model parameters will be much larger, on the order of several dozen. The majority of parameters are needed to describe the pre-thermal stage, which is poorly known. For example, in Ref. [361] ve parameters were used to describe the initial state of the hydrodynamic evolution at a single beam energy. These included a weight between two saturation models, the dependence on having asymmetric thickness functions, the energy density scale, the initial transverse ow, and the initial anisotropy of the stress-energy tensor. The Beam Energy Scan covers a wide variety of energies, plus at each energy one must also model the rapidity dependence of both the energy and baryon densities.

Bayesian analyses follow a fairly standard procedure:

- 1. Distill the data to a list of observables. This may involve reducing numerous graphs to a few numbers using principal component analysis as a guide. By applying a principal component analysis (PCA), one can identify linear combinations of observables which are insensitive to the change of parameters. The original observables, scaled by their variances, . One then constructs a covariance matrix, , where the averaging is performed over several hundred model runs throughout the model space. One then chooses linear combinations of that are eigenstates of . The observables are thus represented by these principal components , which are characterized by the corresponding eigenvalues of , . The combinations with larger eigenvalues, 1, vary signi cantly throughout the parameter space, and thus provide signi cant resolving power. Those with 1 are e ectively useless, and can be ignored in the next two steps. Typically, for applications in heavy-ion physics, the number of signi cant principal components is smaller than the number of model parameters. Thus, Bayesian analyses in heavy-ion physics are typically underconstrained problems despite the immense size of the experimental data set.
- 2. A model emulator must be designed and constructed for use in the Markov-Chain Monte Carlo (MCMC) procedure described below. The purpose of an emulator is to provide the ability to estimate the observables coming from the model, or the principal components, as a function of the model parameters quickly, without having to always run the full model. The emulator is built by running the full model several hundred, or perhaps a few thousand, times semi-randomly throughout the parameter space. These could be the same runs used in (1) to determine the principal components. The

emulator e ectively provides an interpolation from the full-model evaluations, giving

() (). The emulator then takes the place of the full model in the MCMC procedure described below. Gaussian Process emulators are popular [218], but given the smooth, usually monotonic, response of observables to parameters in these applications, one can use various linear or quadratic—ts just as well.

3. The MCMC procedure provides a weighted walk through parameter space. At each step, the likelihood is calculated,

$$\mathcal{L}(\) = \exp \left[\left[\left(\ \right) \right] 2 \right]$$
 (36)

Here, refer to linear combinations of observables, which after being scaled by their uncertainty, are chosen according to PCA. In order to calculate the likelihood at a given point , one must either run the full model to determine , or use an emulator to estimate . Typically a metropolis algorithm is applied. This generates a set of points that represents the posterior probability. The algorithm typically represents millions of such points. The mean value of the parameters are then calculated as

$$=\frac{1}{}^{s} \tag{37}$$

where is the number of points sampled. Other moments of the posterior parameter distribution can be similarly extracted from the MCMC trace.

BEST s statistical analysis is based on that developed by the MADAI Collaboration (Modeling and Data Analysis Initiative), see [218] and [365]. The MADAI toolset assists with building and designing an emulator, and performing the MCMC trace. The software also includes code for analyzing the resolving power of speci c observables in regards to constraining a given parameter [362].

Performing a global Bayesian analysis on BES data is signicantly more challenging than similar analyses at higher energies. The physics, especially the initial stage, is far more uncertain and will likely involve more than twice as many model parameters. In addition to that, the data cannot be modeled using a boost invariant, two-dimensional, approximations of the three-dimensional hydrodynamic evolution. This means that the work is numerically 1-2 orders of magnitude more demanding than any analysis previously performed in this

eld. As the full end-to-end model components were assembled in late 2020, the BEST Bayesian analysis will appear no sooner than late 2021.

Over the last ve years the BEST Collaboration has made tremendous strides towards developing a dynamical framework for a quantitative description of heavy ion collisions at energies relevant to the RHIC beam energy scan. Most of the essential elements the BEST Collaboration set out to address have been addressed:

- A model for complex initial conditions considering baryon stopping and the nite time interval for the transition to hydrodynamics has been developed, implemented and tested by comparing with available experimental data.
- Viscous hydrodynamics has been extended to propagate the relevant conserved currents and their respective dissipative corrections. Also, the time evolution of anomalous currents has been included, and the inclusion of the corresponding dissipative terms is close to completion.
- The time evolution of uctuations has been addressed using both stochastic hydrodynamics as well as a deterministic framework for propagating correlation functions. Within the deterministic approach we have studied the backreaction of uctuations on the hydrodynamic evolution using exploratory calculations in the Hydro+ approach.
- We have constructed a exible model equation of state which contains a critical point in the Ising universality class, and which reproduces available lattice QCD results at vanishing chemical potential. We have implemented this equation of state in a hydrodynamic code.
- The transition from hydrodynamic elds to particle degrees of freedom, often referred to as particlization, has been extended to allow for local conservation of all conserved quantities. This allows for a faithful mapping of uctuations from stochastic hydrodynamics to kinetic theory. In addition, considerable progress has been made towards mapping the correlation functions in the deterministic approach to particles.

- The kinetic evolution of the hadronic phase has been extended to allow for mean eld interactions between the particles. This allows for a non-trivial EOS in the hadronic phase, and for a proper mapping of the EOS used in hydrodynamics to the hadronic phase. To this end a exible density functional model has been developed.
- A Bayesian analysis framework has been adjusted and modi ed to the needs for a comprehensive data comparison with the soon to be expected data from BESII.

While the entire framework is not complete as of this writing, some parts of it have already been used extensively. For example, hydrodynamics including anomalous currents, the AVFD model, is being used by the STAR Collaboration to test the sensitivity of the various observables considered for the analysis of the isobar run. In addition parts of the current framework have been utilized to provide a baseline for the isobar run, which does not include any anomalous currents but accounts for background e ects such as momentum and local charge conservation. The following points need to be elucidated in order to complete the dynamical framework

- Extend the hydrodynamic code to include the Hydro+ framework for the propagation of the two-point functions, necessary for the deterministic description of uctuations. In addition, the transition from Hydro+ to particle degrees of freedom needs to be addressed. Both of these points are presently under development.
- The EOS with a critical point needs to be extended to allow for higher baryon densities. Also, the rst order co-existence region including the unstable spinodal region needs to be modeled. This also requires the inclusion of nite range (or derivative) terms in the EOS.
- The mean eld for the kinetic description needs to be chosen such that it matches the EOS used in hydrodynamics at particlization. This requires also an e-cient algorithm to allow a exible choice of the EOS in the Bayesian analysis.
- The propagation of the anomalous currents (AFVD) needs to be extended to be able to deal with systems at the lowest energies by properly including baryon currents and initial conditions for the axial charges.

• In order to consider third and fourth order cumulants of the baryon number, the Hydro+ formalism needs to be extended to include three- and four-point functions.

Of course the ultimate goal is to carry out a Bayesian analysis of the experimental data to constrain the model parameters and thus the possible existence and location of a QCD critical point as well as the presence of anomalous transport. The rst step of such an analysis is to constrain model parameters by comparing with a set of physical measurements which are not sensitive to either CP nor to anomalous transport, such as spectra and ow. This will reduce the parameter space for the nal comparison including uctuations and correlation observables.

After this work was submitted the rst data from the RHIC isobar run appeared [366].

This material is based upon work supported by the U.S. Department of Energy, O ce of Science, O ce of Nuclear Physics, within the framework of the Beam Energy Scan Theory (BEST) Topical Collaboration, and under contract numbers DE-FG88ER40388 (D.K.), DE-SC0012704 (D.K., S.M., B.S.), DE-SC0018209 (H.U.Y.), DE-SC0020633 (J.N.) DE-FG0201ER41195 (M.S., H.U.Y., S.L., X.A., M.P.), DE-SC0004286 (L.D., U.H., M.M.), DE-AC02-05CH11231 (V.K., V.V.), DE-FG02-03ER41259 (S.P.), DE-SC0013460 (C.S.), DE-SC0021969 (C.S.), DE-SC0020081 (V.S.), DE-FG02-03ER41260 (T.S., M.M.), DE-SC0011090 (K.R., G.R., R.W., Y.Y.), DE-FG02-87ER40328 (M.S.), and O ce of Science National Quantum Information Science Research Centers under the Co-design Center for Quantum Advantage award (D.K.), and in part by the U.S. National Science Foundation Grant numbers PHY-1913729 (J.L.), PHY-2012922 (C.S.), PHY-1654219 (C.R.), and within the framework of the JETSCAPE Collaboration under Award No. ACI-1550223 (U.H.), and in part by the Natural Sciences and Engineering Research Council of Canada (C.G., S.S., M.S.), and in part by the program Etoiles montantes en Pays de la Loire 2017 (M.B., M.N.). U.H. also acknowledges support by a Research Prize from the Alexander von Humboldt Foundation, and V.V. received support by the Alexander von Humboldt Foundation through the Feodor Lynen Program. S.S. and M.S. also acknowledges the Fonds de recherche du Quebec - Nature et technologies (FRQNT) through the Programmede Bourses d'Excellencepour Etudiants Etrangers (PBEEE) scholarship. Y.Y. is supported by the Strategic Priority Research Program of Chinese Academy of Sciences. D.M. is supported by National Science Foundation Graduate Research Fellowship Program under Grant No. DGE 1746047. P.P. acknowledges support by the DFG grant SFB/TR55 and by the Federal Ministry of Education and Research (through BMBF projects 05P18PXFCA and 05P21PXFCA) This research used resources of the National Energy Research Scienti c Computing Center, which is supported by the O ce of Science of the U.S. Department of Energy under Contract No. DE-AC02-05CH11231, resources provided by the Open Science Grid [367, 368], which is supported by the National Science Foundation award 2030508, resources provided by the Ohio Supercomputer Center (Project PAS0254) [369], and resources of the high performance computing services at Wayne State University.

https:

//www.bnl.gov/physics/best/resources.php

https://edms.cern.ch/document/1075059

_ _